[AMERICAN JOURNAL OF SCIENCE, VOL. 291, MARCH, 1991, P. 201–257]

American Journal of Science

MARCH 1991

POROSITY EVOLUTION AND FLUID FLOW IN THE BASALTS OF THE SKAERGAARD MAGMA-HYDROTHERMAL SYSTEM, EAST GREENLAND

CRAIG E. MANNING* and DENNIS K. BIRD
Department of Geology, Stanford University,
Stanford, California 94305

ABSTRACT. **Deformation and heat transfer associated with the Skaergaard intrusion caused a meteoric hydrothermal system in the fractured gabbros and their basaltic host rocks. In the basalts, fluid migration accompanied contact metamorphism and occurred in a network of macroscopic structures which included primary pores, hydrothermal breccias, and fractures. These pore structures record the changes in stress, temperature, permeability, and mineral reactions associated with fluid flow in the evolving hydrothermal system.**

The earliest pore type was primary open space associated with basaltic lava flows. Average cumulative macroscopic porosity was greater in brecciated aa units (11 percent) than in interlayered massive lavas (4 percent), indicating that the country rocks into which the Skaergaard was emplaced were characterized by stratigraphically controlled units of contrasting porosity. After emplacement of the intrusion, prograde metamorphism of basalts near the intrusion produced three mineral zones: the *olivine zone* (0–10 m from the contact), the *pyroxene zone* (10–210 m), and the *actinolite + chlorite zone* (>210 m). Fracture systems associated with prograde metamorphism are horizontal and parallel to bedding at distances >150 m from the contact but range from horizontal to vertical within 150 m. These fractures probably formed by pore fluid expansion during heating of the aureole. Synchronous hydrothermal breccia zones formed at the margins of contact-parallel, pre-Skaergaard dikes. Together with the primary porosity, these pores hosted the migration of hydrothermal fluids during prograde metamorphism. The orientations of pores of this type resulted in upward migration of hydrothermal fluids in a 150-m-wide zone along the contact and horizontal migration of fluids toward the intrusion beyond 150 m. Later vertical veins formed after crystallization of the intrusion in response to contraction of the cooling gabbros and emplacement of mafic dikes. The vertical veins provided the conduits for further lateral and vertical fluid migration that caused local retrograde alteration of the metabasalts. Cumulative macroscopic porosities associated with prograde metamorphism were at least an order of magnitude greater than those associated with retrograde alteration, indicating that

* Present address: Department of Earth and Space Sciences, University of California Los Angeles, Los Angeles, California 90024

the quantities of fluid in these rocks were greatest early in the system's history. The evolution of porosity and fluid flow during contact metamorphism in the Skaergaard magma-hydrothermal system reflects systematic interrelationships among a changing state of stress, magma emplacement and crystallization, heat transfer and associated changes in fluid pressure, and mineral precipitation in the pores.

INTRODUCTION

The emplacement of magma redistributes heat in the Earth through the transport of thermal energy from the cooling igneous body into its host rocks. Contact metamorphic rocks surrounding intrusions, subaerial and submarine geothermal systems, and a wide variety of hydrothermal ore deposits attest to the contribution of circulating fluids in this heat transport. Numerical simulation of the relationships between rock deformation, metamorphism, fluid flow, and chemical mass transfer in these magma-hydrothermal systems shows that variations in magma and pore-fluid pressure during heat transfer lead to rock fracture and an interconnected pore network in the host rocks near the intrusive contact (Norton and Knight, 1977; Norton, 1979, 1984; Knapp and Norton, 1981; Delaney, 1982). In response to thermally induced density gradients, fluids migrate through this pore space with pathlines controlled by the geometry of the pore network and by the spatial and temporal variations in permeability.

These observations illustrate that understanding fluid migration in field exposures of contact metamorphic rocks requires characterization of the distribution and evolution of porosity. Spatial and temporal changes in the pore network make the hydrology of contact metamorphism complex. For example, field and laboratory studies of this environment suggest that different lithologies may enhance or retard the migration of fluids (Hover-Granath, Papike, and Labotka, 1983; Nabelek and others, 1984; Ferry, 1987, 1988, 1989) and that the geometry of the pore network and the volume change in space and time (Holness, Bickle, and Harte, 1989; Manning, ms; Manning and Bird, 1991). In addition, a wide variety of pore structures can host fluids during contact metamorphism. Because of their macroscopic connectivity, mineral-filled fractures (veins) have received much attention in studies of porosity and permeability evolution associated with intrusions (Villas and Norton, 1977; Titley, 1978; Haynes and Titley, 1980; Norton, Taylor and Bird, 1984; Bird, Rogers, and Manning, 1986; Titley and others, 1986; Nehlig and Juteau, 1988). These investigations show that the structure and mineral filling of the pore network record the time-space evolution of fluid flow in magma-hydrothermal systems. However, none of these studies integrates the evolution of a pore network with contact metamorphic history to characterize the timing and geometry of fluid flow at the margins of an intrusion.

In this paper, we describe the evolution of porosity and fluid flow in the contact metamorphosed, basaltic host rocks of the Skaergaard magma-

hydrothermal system in central East Greenland. This locality is ideal for such a study because the hydrothermal system associated with the cooling of the intrusion is well understood through studies of hydrothermal veins (Norton, Taylor, and Bird, 1984; Bird, Rogers, and Manning, 1986; Bird, Manning, and Rose, 1988; Manning and Bird, 1986) and patterns of ^{18}O depletion in magmatic minerals (Taylor and Forester, 1979; Norton and Taylor, 1979). The observed distribution of $^{18}O_{plagioclase}$ depletion requires that the basalt host rocks were the fluid source region in this system and had high time- and volume-averaged permeabilities (Norton and Taylor, 1979). We have therefore conducted detailed field and laboratory investigations of the basalts, both in the immediate vicinity of the contact (this study and Manning and Bird, 1990, 1991) and throughout the region (Bird and others, 1991), to characterize the geologic record of fluid flow in the recharge portion of this Early Tertiary hydrothermal system. Here, we describe five different pore types in the contact aureole of the Skaergaard intrusion, and we relate the formation of these pore types to the volcanic environment and structural evolution of the system. When combined with measurements of pore density and macroscopic, cumulative porosity of each pore type, this information leads to a detailed understanding of the geometry and evolution of fluid flow at the margins of the Skaergaard intrusion.

GEOLOGIC BACKGROUND

Regional Geology

The Skaergaard intrusion and its host basalts were emplaced during the initial stages of rifting of the North Atlantic ocean basin (Nielsen, 1978; Brooks, 1980; Brooks and Nielsen, 1982a). As summarized by Brooks and Nielsen (1982b), rifting began in the Kangerdlugssuaq region of central East Greenland (fig. 1) with the development of a Late Cretaceous, fault-controlled basin in Archaean gneissic amphibolites (Leeman, Dasch, and Kays, 1976; Kays, Goles, and Grover, 1989). Late Cretaceous to Late Paleocene arkosic sandstones and shales unconformably overlie the basement lithologies. These sedimentary rocks are in turn succeeded by a thick sequence of mafic volcanics which have been divided into, in order of oldest to youngest, the Lower Basalts (Vandfaldsdalen and Mikis formations), the Main Tuffs (Haengefjeldet Formation), and the Plateau Basalts (Irminger Formation; Wager, 1934, 1947; Soper and others, 1976a,b; Nielsen and others, 1981). The onset of extrusive volcanism is estimated to have been at ~57 my ago (Ma). Subsequent emplacement of east-west-trending tholeiitic dikes of the coastal dike swarm was followed by intrusion of the Skaergaard and related dikes and sills (fig. 1) at 55 Ma (Brooks and Gleadow, 1979). During the next 2 to 5 my, continued east-west dike emplacement and associated faults caused tilting of the stratigraphy to the south. Later activity included the emplacement of late alkaline dikes and intrusions and domal uplift (Brooks, 1979; Brooks and Nielsen, 1982b; Noble, Macintyre, and Brown, 1988).

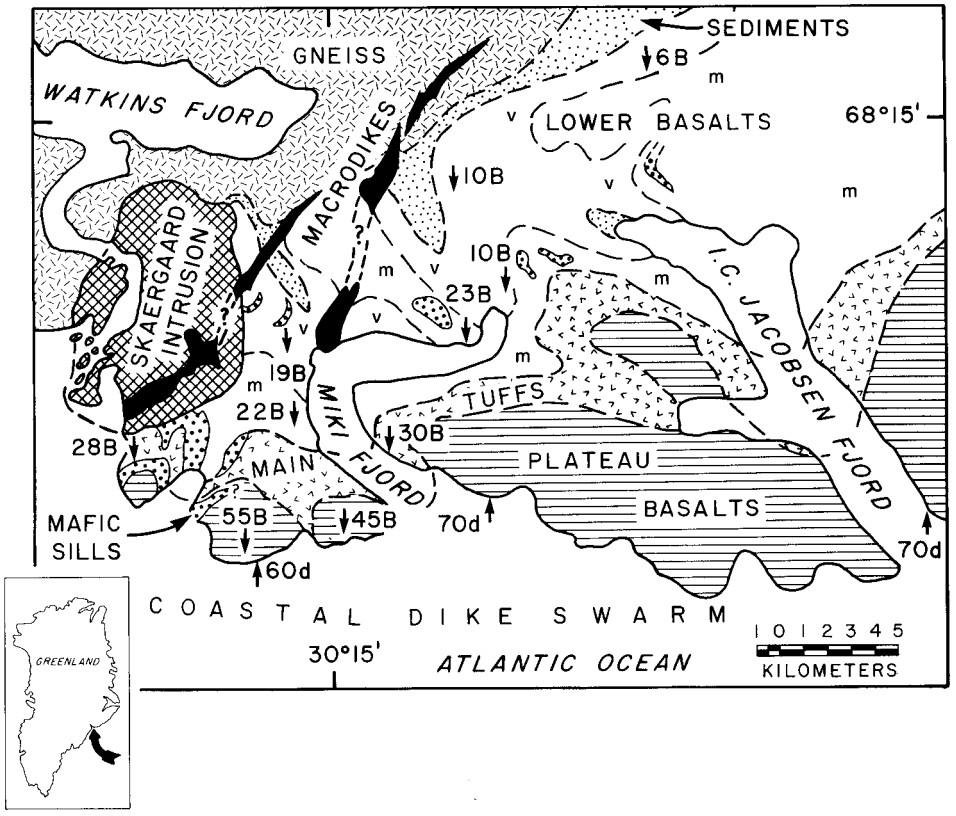

Fig. 1. Geologic map of the region near the Skaergaard intrusion. The Tertiary stratigraphy includes, in order of oldest to youngest: clastic sediments (fine stippled pattern); the Lower Basalts consisting of the Vandfaldsdalen (v's) and Mikis (m's) formations; the Main Tuffs (random v pattern); and the Plateau Basalts (ruled pattern). The basalts strike east-west and dip to the south (dip directions shown with arrows labelled "B"). Dikes of the Coastal Dike Swarm strike east-west and dip steeply to the north (dip directions shown with arrows labelled "d"). Also shown are mafic sills (coarse stippled pattern). The sills are generally concordant with the Tertiary stratigraphy and predate Skaergaard emplacement. The inset shows the location of the map in Greenland.

Geology of the Skaergaard Intrusion

The Skaergaard gabbros (fig. 2) are tholeiitic and are characterized by extreme iron enrichment (Wager and Deer, 1939; Wager and Brown, 1967). The earliest exposed crystallization products are the Marginal Border Group gabbros along the walls of the intrusion. Based on macroscopic textural variations, these rocks have been subdivided into two zones: the Tranquil Division, consisting of fine-grained granoblastic chilled marginal gabbro, perpendicular feldspar gabbros, and patchy pyroxene gabbros, and the Banded Division consisting of coarse-grained gabbros with contact-parallel layering (Wager and Deer, 1939; Wager

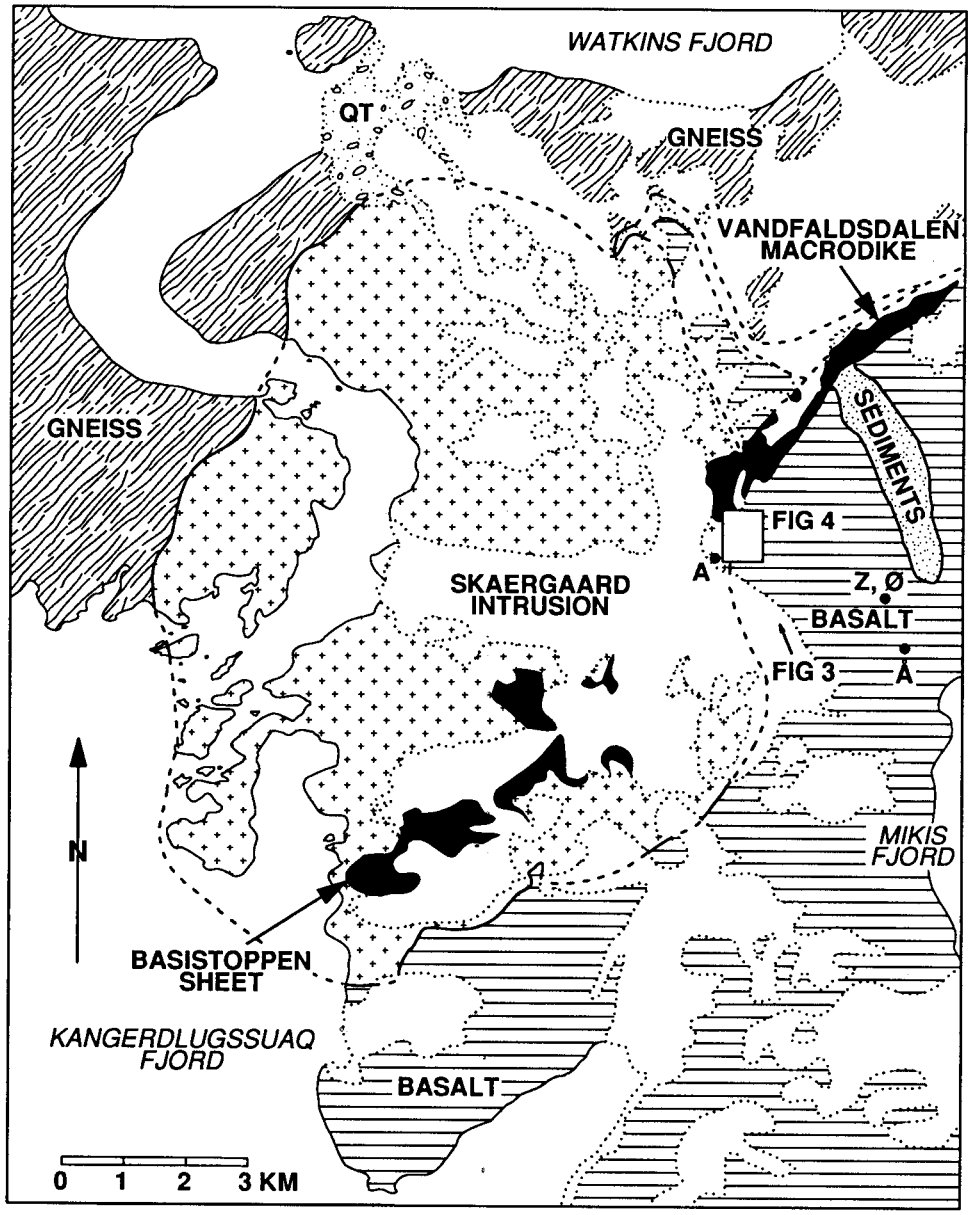

Fig. 2. Geologic map of the Skaergaard intrusion and its country rocks, modified after Bird, Rogers, and Manning (1986). QT denotes talus deposits. Also shown are the point from which the photograph in figure 3 was taken and the location of figure 4. Localities labelled A, Z, Ø, and Å are pore survey stations discussed in the text.

and Brown, 1967; Hoover, 1989a,b). Within the chamber the magma crystallized from the bottom upward to form the Layered Series and from the top downward to form the Upper Border Group (Wager and Deer, 1939; Naslund, 1984; McBirney and Noyes, 1979; McBirney, 1989).

Norton, Taylor, and Bird (1984) suggest that the Skaergaard magma was injected through pipe-like feeders in the gneisses and formed a sill by spreading laterally along the unconformity between the basement gneisses and the Tertiary strata. Continued magma influx uplifted the basaltic overburden as the chamber evolved into a laccolith. The stratigraphy at the eastern contact (figs. 3 and 4) is clearly truncated against the gabbro

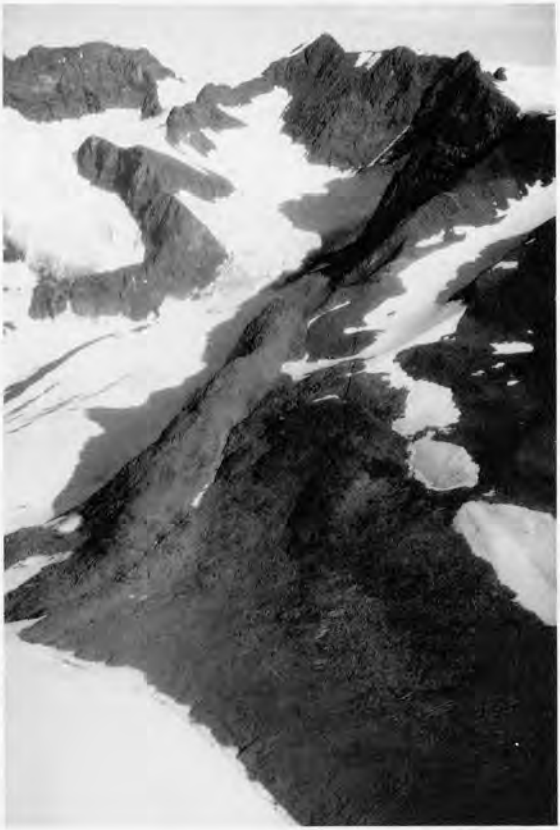

Fig. 3. Oblique aerial photograph of the study area. View is to the north-northeast (see fig. 2). The ridge in the center of the photo consists of Marginal Border Group gabbros of the Skaergaard intrusion. The contact lies in the gully between the light-weathering gabbros and dark-weathering basalts in the foreground. Basalts are exposed to the east of the gully; the right margin of the photograph is ~500 m from the contact. The mountains in the background are the Layered Series gabbros.

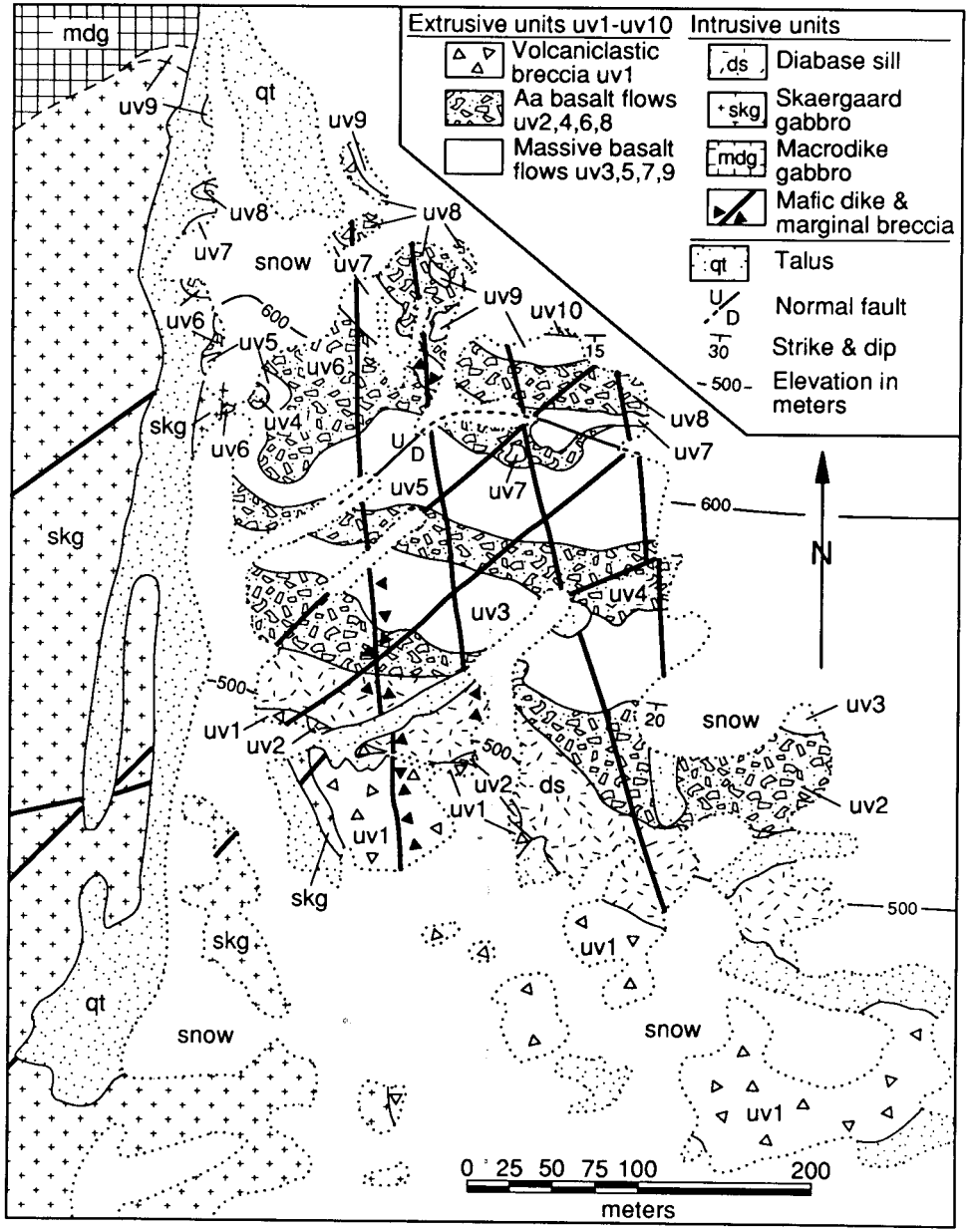

Fig. 4. Geologic map of the study area. See figure 2 for location. Individual flow units of the Upper Vandfaldsdalen Formation are designated *uv1* to *uv10*, with numbers increasing upsection. The units were differentiated on the basis of massive and brecciated textures (see text).

and shows little evidence of deformation, suggesting that the final stages of chamber inflation involved piston-like uplift and faulting of the host rocks. Mechanical considerations require that magma injection rate was sufficiently rapid that the chamber filled to its final volume of ~190 km^3 in several hundred years (Norton, Taylor, and Bird, 1984). Norton and Taylor (1979) suggest that the magma had completely crystallized by ~130,000 yrs after emplacement and that the system had cooled to near-ambient conditions after ~500,000 yrs.

During subsolidus cooling, brittle deformation led to the formation of four fracture types, including gabbro pegmatites, hydrothermal veins, transgressive granophyres, and mafic dikes (Norton, Taylor, and Bird, 1984; Bird, Rogers, and Manning, 1986; Hirschmann, 1987, 1988; Rogers and Bird, 1987; Bird, Manning, and Rose, 1988). The large volume decrease associated with the change from tholeiitic liquid to solidified gabbro was in part accommodated by emplacement of subhorizontal gabbro pegmatites. These structures are crosscut by the earliest hydrothermal veins, which began forming when temperatures in the gabbros were 600° to 900°C (Manning and Bird, 1986). These veins are locally crosscut by granophyres and were sealed by hydrothermal minerals at 500° to 600°C. Later hydrothermal veins formed below 500° to 600°C and have orientations and distributions that suggest that they were related to later structural or intrusive features such as faults, granophyres, and mafic dikes (Bird, Manning, and Rose, 1988). The hydrothermal veins provided the permeable conduits for the influx of meteoric water that caused widespread ^{18}O depletion of the magmatic phagioclase (Taylor and Forester, 1979) and transported ~20 percent of the thermal energy from the intrusion into the host rocks (Norton and Taylor, 1979).

GEOLOGY OF THE SKAERGAARD EAST CONTACT

Basalts

The Skaergaard magma intruded basalts, gneisses, and volumetrically insignificant sedimentary rocks (fig. 2), all of which are contact metamorphosed near the intrusion (Wager and Deer, 1939; Myers, 1976; Bird and others, 1985, 1986; Manning, ms). Norton and Taylor (1979) found that the $\delta^{18}O_{plagioclase}$ distributions in the Skaergaard gabbros could be reproduced numerically by assuming time- and volume-averaged permeabilities of 10^{-11} cm^2 in the basalts and 10^{-16} cm^2 in the gneisses. The substantial contrast in permeability necessary to explain the ^{18}O exchange in the gabbros indicates that the evolution of the hydrothermal system was strongly controlled by the hydrologic character of the basalt host rocks and that virtually all the water in the hydrothermal system flowed through the basalts (Norton and Taylor, 1979). Our investigation of porosity evolution in the host rocks was therefore limited to the basaltic lithologies.

The eastern contact between the Skaergaard intrusion and the basalts (figs. 3 and 4) was chosen for detailed study because of its extensive, accessible exposures and because modification by later dikes

and sills is minor. Lithologies in this 0.35 km^2 study area include volcanic breccias and vesicular flows of the upper Vandfaldsdalen formation, a diabase sill, and vertical diabase dikes with a variety of orientations (fig. 4). The study area lies on a steep south-facing slope (fig. 3), and the strata strike approx east-west and dip 10° to 30° to the south (fig. 4). Thus the map view in figure 4 is also an oblique cross section of the contact aureole. The depth of the map area at the time of Skaergaard magma emplacement was 4 ± 1 km (Nielsen and others, 1981; Brooks and Nielsen, 1982b), and the study area corresponds to the stratigraphic level of the Middle Zone of the Layered Series, although exposures of the Skaergaard intrusion in this area are all within the Tranquil Division of the Marginal Border Group.

Primary volcanic features such as vesicles and breccia zones are preserved to the highest grades of metamorphism (Manning, ms), allowing identification of ten extrusive units, *uv1* to *uv10*, which represent individual flows or groups of flows of the same textural type. Units *uv1* to *uv10* comprise the lower ~70 percent of the upper Vandfaldsdalen formation and, with the exception of *uv1* (see below), are uniformly tholeiitic in composition (Manning, ms).

The lowermost unit (*uv1*) is a polymict, matrix-supported, volcaniclastic breccia (main breccia of Wager, 1934; unit μ of Nielsen and others, 1981) which defines the base of the upper Vandfaldsdalen formation (fig. 4). As noted by Soper and others (1976a), clasts of massive volcanics, pillow fragments, and breccia are up to 0.5 m in the largest dimension and occur in a fine-grained matrix of basaltic detritus with abundant augite and plagioclase fragments. *Uv1* is compositionally heterogeneous, containing clasts of picrites, tholeiites, basaltic andesites, and ankaramites of the lower Vandfaldsdalen formation.

Interbedded, massive,[1] vesicular basaltic lava flows and monomict basaltic breccia overlie *uv1*. The four massive flow units (*uv3*, *5*, *7*, and *9*) are up to 10 m thick and fine-grained. Vesicles and irregular cavities (fig. 5A) increase in abundance toward flow tops.

Monomict breccias can be distinguished from massive lavas and the polymict breccia by the presence of angular clasts of fine-grained basalt in a matrix of varying proportions of basaltic detritus, secondary minerals, and open space (fig. 5B, C). In the study area the five monomict breccia units (*uv2*, *4*, *6*, *8*, and *10*) are up to 15 m thick. Units *uv2* and *uv8* have massive, unbrecciated, nonvesicular centers 5 to 10 m thick. The monomict breccia units are interpreted as aa flows based on their similarity to Hawaiian aa described by Wentworth and Macdonald (1953) and Macdonald (1967).

Mafic Dikes and Sills

Emplacement of sills and dikes both predated and postdated the Skaergaard intrusion (Nielsen, 1978). Crosscutting relations between

[1] The term "massive" is used to differentiate unbrecciated from brecciated lavas. Massive, unbrecciated units contain variable vesicle contents.

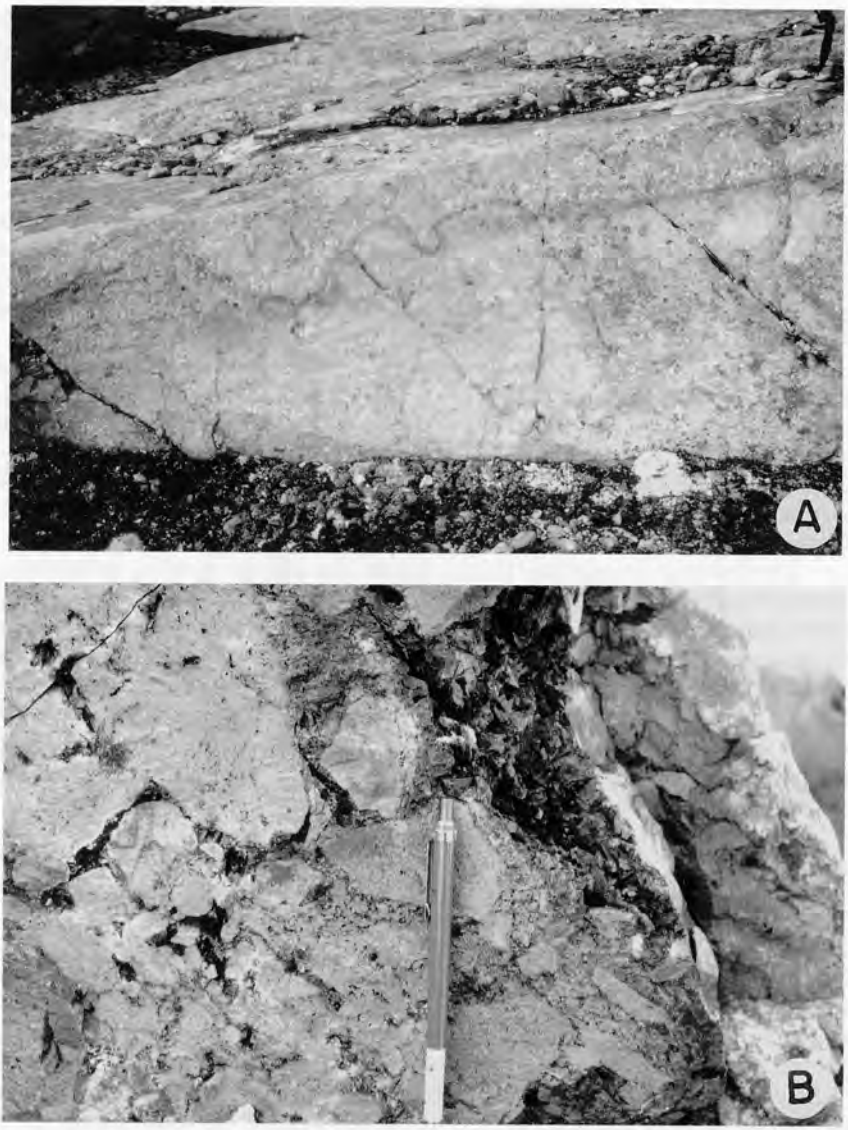

Fig. 5(A) Boundary between two massive basalt flows ~700 m east of the study area. The dark zone between the flows is the oxidized, hematite-rich top of the underlying flow. The left side of the photograph illustrates the commonly observed concentration of vesicles near the top of massive flows. Field of view is ~2 m wide. (B) Macroscopic texture of brecciated portion of aa flow *uv2* 500 m east of the contact. Note the abundant primary porosity in interspace between clasts. This pore space is now filled by quartz, actinolite, chlorite, and calcite. Pencil is 14 cm long. (C) Photomicrograph showing mineral-filled interspace between clasts in aa flow from the *pyroxene zone* 40 m east of the contact. The earliest phase to precipitate was clinopyroxene, and the subhedral clinopyroxene terminations are interpreted as evidence for growth into open pore space. This pore space is now filled by altered K-feldspar and quartz, which probably formed along with the quartz + feldspar veins (see text). Nicols partly crossed. Field of view is 3 mm wide.

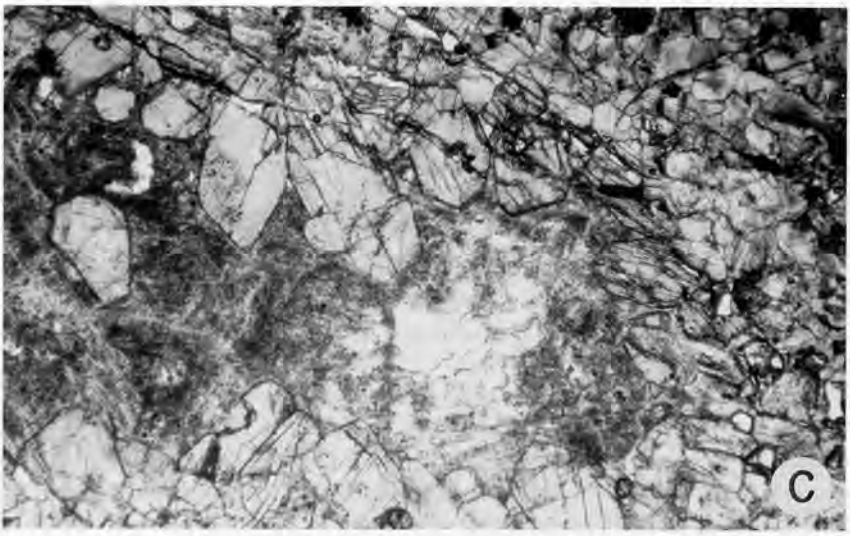

Fig. 5 (continued)

these intrusive units allow determination of their relative ages. The earliest intrusive unit in the map area is a fine-gained 10- to 15-m-thick mafic sill (*ds*, fig. 4) emplaced between the polymict breccia (*uv1*) and the overlying aa (*uv2*). The sill and the extrusive units were in turn crosscut by several north-northeast- to north-south-trending mafic dikes (fig. 4), which will be referred to as north-south dikes for brevity. The north-south dikes and the sill are characterized by recrystallized, metamorphic textures and mineral assemblages identical to those of adjacent basalts (see below), and the sill is crosscut by the Skaergaard intrusion (fig. 4). These observations indicate that both units were intruded prior to Skaergaard emplacement.

The northeast-trending Vandfaldsdalen macrodike (figs. 2 and 4) is ~500 m wide in the east contact region and crosscuts the Skaergaard (Deer, 1976; Bird and others, 1985; Rosing, Lesher, and Bird, 1989; White and others, 1989). Field relations suggest that the dike is contiguous with the Basistoppen sill (Douglas, 1964; Naslund, 1986, 1989). The presence of partially melted Skaergaard gabbros at the basal contact of the sill (Naslund, 1986) and abundant, high-temperature calcic amphibole veins in both the Basistoppen and Skaergaard lithologies (Bird, Manning, and Rose, unpublished data) require emplacement of the sill when the Skaergaard gabbros were solidified but still at elevated temperatures. Metamorphic recrystallization associated with the Vandfaldsdalen macrodike are limited to < 10 m from the dike margin and do not affect the Skaergaard-related metamorphic mineral zonation in the basalts in the area of figure 4. A suite of vertical mafic dikes subparallel to the Vandfaldsdalen macrodike represents the youngest intrusive unit in

the study area. These dikes occasionally display left-lateral offsets of the lavas and the Skaergaard contact of up to ~1 m (fig. 4). Compilation of dike orientations over 3 km^2 east of the contact (fig. 6) shows that, although not found in the area of figure 4, northwest- and east-west-trending dikes also occur in the region.

Metamorphic History of the Skaergaard East Contact

Heat transfer from the cooling Skaergaard intrusion led to metamorphic recrystallization and the development of three metamorphic mineral zones in the study area (Manning, ms; Manning and Bird, 1991): the *actinolite + chlorite zone* (210 m from the contact), the *pyroxene zone* (10–210 m), and the *olivine zone* (0–10 m). The mineralogy of each zone is summarized in figure 7. Diagnostic minerals or textures include olivine in the *olivine zone,* coexisting clinopyroxene and orthopyroxene in the *pyroxene zone,* and actinolite and chlorite replacing magmatic clinopyroxene in the *actinolite + chlorite zone.* Textures of hornfels from the *pyroxene* and *olivine zones* are distinct from those in the *actinolite + chlorite zone* in that the former are characterized by granoblastic-polygonal textures with grain size increasing toward the contact, whereas the latter display relict igneous textures. Similar assemblages are found in the basalts that host the Cuillin gabbros on the Isle of Skye, Scotland (Ferry, Mutti, and Zuccala, 1987).

Peak metamorphic temperatures ranged from ~1000°C in the *olivine zone* to 300° to 550°C in the *actinolite + chlorite zone* (Manning, ms; Manning and Bird, 1991). We interpret the maximum temperatures

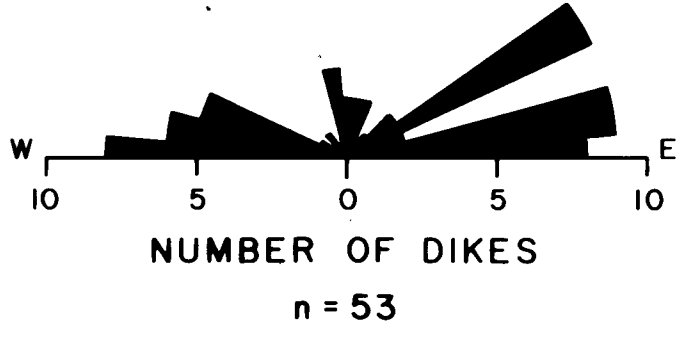

Fig. 6. Rose diagram showing the orientation of 53 dikes in the basalts east of the Skaergaard intrusion. The diagram is oriented with north to the top. Dike orientations were determined from an oriented, vertical aerial photograph centered near the point labelled "Z,ϕ" in figure 2. The sample area covered by the photograph is ~3 km^2. Ground observations indicate that all dikes dip within 15° of vertical in this region.

recorded at any given distance from the gabbro-basalt contact, the locations of the mineral zones, and the metamorphic textures associated with them as representing prograde thermal metamorphism, where "prograde" signifies metamorphism associated with increasing temperature. The distribution of peak metamorphic temperatures in the aureole reflects the combined effects of conductive and convective heat transport and is discussed in a separate study (Manning and Bird, 1991). In the outer portion of the *pyroxene zone* and near later fractures in both the *pyroxene* and *olivine zones,* the prograde mineral assemblages are locally crosscut or overgrown by *actinolite + chlorite-zone* assemblages (fig. 7). The

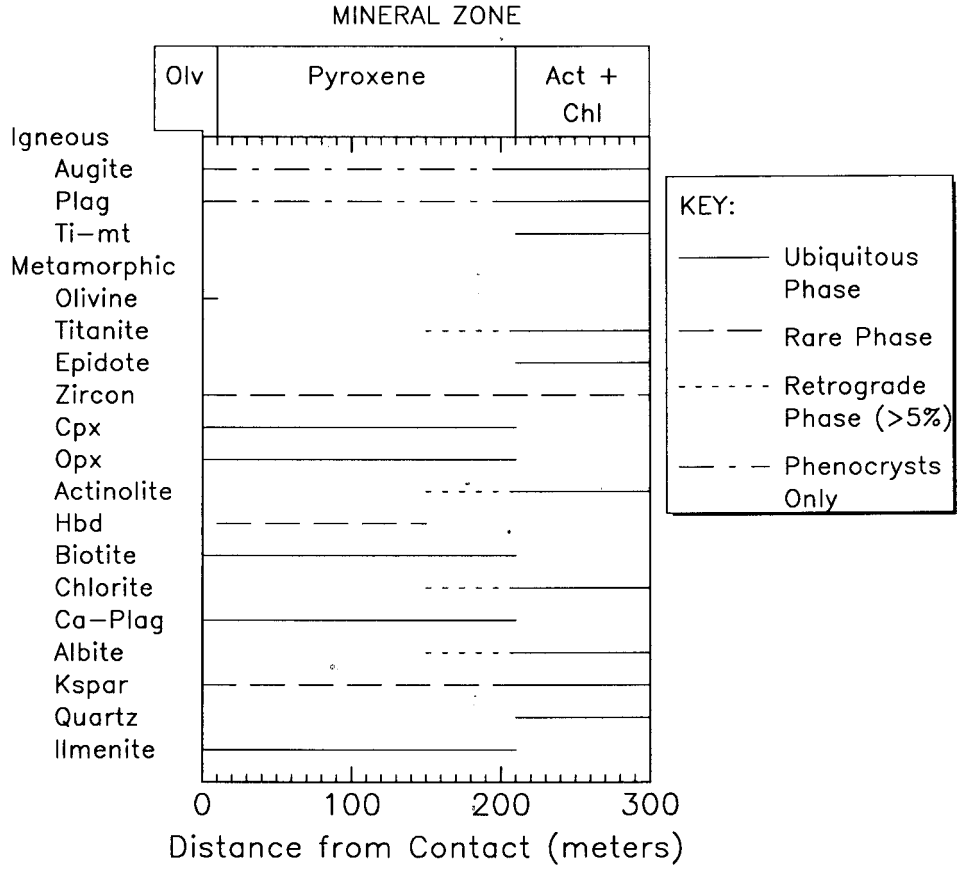

Fig. 7. Summary of mineral parageneses in metabasalt matrices from the study area (from Manning, ms). Pore-filling minerals are not included. Metamorphic mineral zones shown across the top of the diagram include the *olivine zone* (olv), the *pyroxene zone,* and the *actinolite + chlorite zone* (act + chl; see text). Abbreviations: Plag, plagioclase; Ti-mt, titanian magnetite; Cpx, calcic clinopyroxene; Opx, orthophyroxene; Hbd, hornblende, Ca-plag, calcic plagioclase; and Kspar, potassium feldspar.

actinolite + chlorite-zone assemblages (300°–550°C) record lower temperatures than those they cross cut (700°–1000°C), and we therefore refer to the process that produced them as retrograde metamorphism.

In their simulation of the heat transfer and oxygen isotope exchange during cooling of the Skaergaard intrusion, Norton and Taylor (1979) predicted temperatures, pressures, and transport properties for discrete grid points on a simplified cross section of the system. These grid points are the centers of rectangles 1 km in the horizontal dimension and 0.56 km in depth, and all calculations associated with the points represent averages over the area of the rectangle. Figure 8 shows the variation in temperature with time after Skaergaard emplacement for the rectangle in the host basalts that includes the projected position of the map area of figure 4. It can be seen in figure 8 that the model predicts that temperatures rose rapidly in this portion of the system in the first 40,000 yrs after emplacement and decreased slowly therafter. Norton and Taylor's calculations suggest that prograde thermal metamorphism occurred in the first 40,000 yrs, whereas retrograde mineral assemblages could have developed at any time after this. The maximum temperature in figure 8

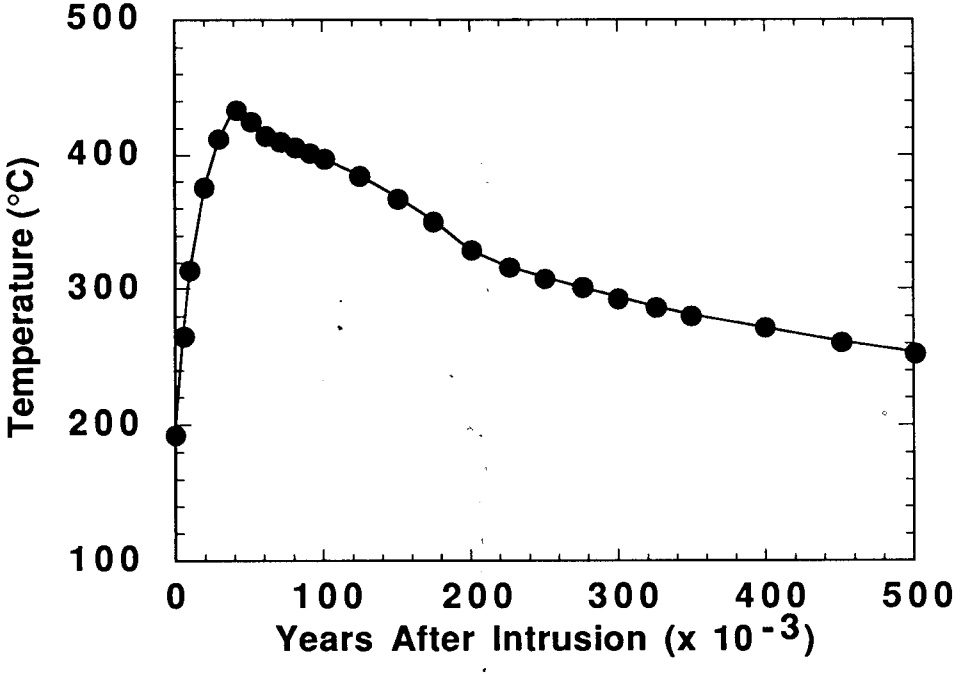

Fig. 8. Temperature versus time for the 0.56 km^2 rectangle including the study area in Norton and Taylor's (1979) numerical model S2. Physical properties of the S2 simulation are used because they led to the best reproduction of the $^{18}O_{plagioclase}$ distribution in the gabbro (Norton and Taylor, 1979).

is lower than peak metamorphic temperatures in the *pyroxene* and *olivine zones* because the temperatures shown in the figure are averages of the 0.56 km^2 area extending to 1 km from the intrusion. The maximum temperature attained at this grid point in the model is consistent with the observation that the *actinolite + chlorite zone,* in which temperatures were 300° to 550°C, extends from 210 to >1000 m from the gabbro-basalt contact (Bird and others, 1991), or ~80 percent of the area to which the average temperatures of figure 8 apply.

MEASUREMENT OF POROSITY

Porosity in Paleo-Flow Systems

Porosity (Φ) is the volume of pore space divided by the volume of rock and pores and varies as a function of pressure, temperature, and time in magma-hydrothermal systems (Moskowitz and Norton, 1977; Walder and Nur, 1984). This parameter is dimensionless and is often multiplied by one hundred and described in percent, a convention adopted in the present study. Because the pore space hosted the fluid phase in paleo-flow systems, investigation of the evolution of the flow system requires quantitative comparison of changes in the distribution and abundance of pores with time. However, two factors make it difficult to determine Φ in these systems: the pore space is typically at least partially filled by secondary minerals, and the rates of pore formation and filling may vary, such that pores grouped together based on similarities in morphology and/or mineral fill did not necessarily form at the same time or open or seal at the same rate. To avoid these problems, we present our measurements of pore abundance as cumulative porosity (Φ^*), which we define for a given pore type as the percentage of sample area occupied by the pore type of interest, filled or unfilled by secondary minerals.

The relationship between Φ^* and Φ is illustrated schematically in figure 9. Figure 9A shows the variation in Φ with time for the simple case of a single fracture episode in which Φ is a continuous function of time (t). Such an event will involve an early stage (t_0–t_1) in which Φ increases, and $\partial\Phi/\partial t > 0$. Time t_1 is defined as the maximum in Φ for any individual pore-forming event. It can be seen that $\partial\Phi/\partial t = 0$ at t_1 for the simple case illustrated in figure 9A. After t_1, porosity decreases due to mechanical closing of the pore or to mineral filling (t_1–t_2, $\partial\Phi/\partial t < 0$). If porosity reduction is due only to mineral filling of the single fracture, figure 9B illustrates that the total porosity produced (Φ_{max}) is equal to Φ when $\partial\Phi/\partial t \geq 0$. When $\partial\Phi/\partial t < 0$, Φ_{max} still corresponds to Φ at t_1. The value of Φ^* for the single fracture episode is thus the value of Φ_{max} at the time of observation (t_{obs}) of the fracture. Figure 9C to D shows the relationships between Φ and Φ^* for pores of other origins. For primary porosity (fig. 9C) the pore-forming event and Φ_{max} are associated with the formation of the rock itself. In this case, Φ^* is again equal to Φ_{max} at t_{obs}. Figure 9D shows a hypothetical set of fractures identified as the same pore type but

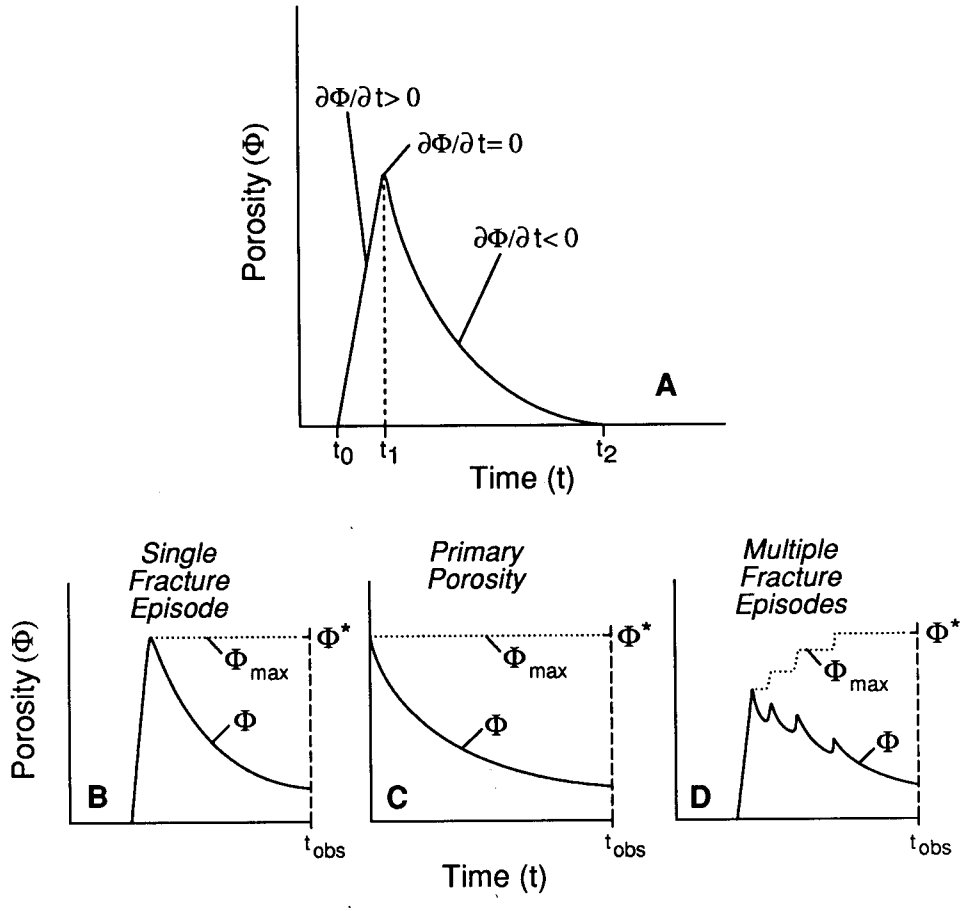

Fig. 9(A) Schematic illustrations of porosity (Φ) versus time (t) for a hypothetical single fracture episode. Porosity is shown as a continuous function of time and increases ($\partial\Phi/\partial t > 0$) from the onset of fracture opening, t_0, to the time at which fracture opening ceases, t_1. At t_1, $\partial\Phi/\partial t = 0$, and after t_1, $\partial\Phi/\partial t < 0$ as Φ decreases due to mineral filling or mechanical closure of the fracture. Below (A) are schematic illustrations of the relationship between Φ and Φ^* for pores of different origins, including a single fracture episode (B), primary porosity (C), and multiple fracture episodes (D). In each case, Φ^* is equal to the total porosity produced (Φ_{max}) at the time of observation (t_{obs}).

representing porosity associated with four fracturing episodes. This figure illustrates that, when pores of the same type formed at different times, Φ_{max} at any time reflects the sum of Φ produced to that time, and Φ^* simply corresponds to Φ_{max} at the time of observation.

In general, a given pore type reflects one or more pore-forming events, each of which is characterized by time intervals in which porosity increases (t_0–t_1, fig. 9A) and time intervals in which Φ decreases (t_1–t_2, fig.

9A). Thus Φ^* can be defined quantitatively for a given pore type at the time of observation as

$$\Phi^* \equiv \sum_{i}^{i^*} \Phi_i^{t_1} - \Phi_i^{t_0} \tag{1}$$

where i denotes each pore-forming event responsible for the generation of a given pore type, and i^* is the number of pore-forming events associated with the pore type at t_{obs}. Note that eq 1 reflects the fact that Φ^* is defined only at one time (t_{obs}) and does not describe the time dependence of Φ_{max}.

Norton and Knapp (1977) discuss the relationship between porosity and fluid flow by identifying three components of the porosity: flow porosity, which is the fraction that constitutes rock permeability and in which mass transport is by fluid advection; diffusion porosity, in which the primary transport mechanism is by diffusion through the fluid; and residual porosity, which represents pores not connected to the flow or diffusion porosity. However, partial filling of pores and uncertainties in the nature of pore connectivity in natural exposures makes it impossible to determine whether the transport of mass that led to mineral precipitation in the pore space was by flow or diffusion. Values of Φ^* (eq 1) thus reflect the sum of flow, diffusion, and residual porosity as defined by Norton and Knapp (1977). Note also that changes in Φ associated with elastic recovery after failure or mechanical closure with changes in stress regime are not recorded by measured Φ^*. Elastic recovery after failure probably did not change Φ significantly because it was likely to have been a transient process associated with the short time intervals during or immediately after pore formation. In addition, textural evidence (see below) supports the conclusion that mechanical closure of fractures was not an important process in porosity reduction.

Measurement of Φ^* in the Study Area

In the basaltic rocks of the study area, macroscopically observable pores such as vesicles, breccia interspace, and veins are voluminous, and measurements of pore abundance and pore size were limited to those pores that could be identified with the unaided eye. Values of Φ^* for irregular pores such as vesicles and breccia interspace were measured by point counting (≥ 1000 points) on sawed surfaces of representative samples ranging in size from 250 to 500 cm^2. For point-count measurements Φ^* (in percent) is calculated using the relation

$$\Phi^* = \frac{n_p}{N} \times 100, \tag{2}$$

where n_p is the number of points counted as pores, and N is the total number of points counted. The macroscopic methods used limit the detectable size of pores of this type to ~ 1 mm. The consequences of limiting pore sizes to > 1 mm in solving eq 2 will be discussed after the

different pore types are described, but it will be seen that the large values of Φ^* for macroscopic pores minimize the uncertainties introduced.

For veins,

$$\Phi^* = d\left(\frac{l}{a_{survey}}\right) \times 100, \quad (3)$$

where d is mean mineralogic vein aperture (in cm) as measured in representative thin sections, l is the sum of all fracture lengths, and a_{survey} is the area surveyed. The quotient l/a_{survey} corresponds to vein density (cm^{-1}) and is measured in the field using the methods outlined by Snow (1969, 1970), Bianchi and Snow (1969), and Titley and others (1986). Because of their continuity, veins with very narrow widths (<0.1 mm) are easily detected. Field survey areas in this investigation ranged from 1 to 45 m^2. These sample sizes were found to be sufficient to characterize the local variability in pore structures, how these features relate to the structural and metamorphic evolution of the country rocks, and the extent to which they record the details of fluid flow throughout the cooling history of the system. It is important to note, however, that much larger sample sizes would be required to characterize fracture-related Φ^* for a representative elemental area. For example, Barton and Hsieh (1989) note that the representative elementary area required to characterize the densely fractured tuffs of Yucca Mountain, Nevada, is so large (>1720 m^2) that cataloguing all fractures is prohibitive.

Uncertainties in Φ^* determined using eqs 2 and 3 can be attributed to the sample size in the point-count determinations and difficulties in measuring vein apertures. Minimum values of N in eq 2 of 1000 lead to uncertainties of ≤1.5 percent (Chayes, 1956). Uncertainties in aperture are difficult to quantify but are attributable to wall-rock alteration, which can lead to anomalously large apertures and variations in apertures between and within samples. Nevertheless, we show below that Φ^* varies between pore types by more than five orders of magnitude, a range of values that certainly exceeds these potential uncertainties.

THE PORE NETWORK

Five different pore types occur in the area of figure 4: primary pores, horizontal veins, net veins, hydrothermal breccias, and vertical veins.[2] To evaluate the distribution, abundance, and timing of pore formation throughout the east-contact region, 28 survey stations were selected at which pore types were identified and described; crosscutting relations, mineral filling, orientation, and length or volume were recorded; and representative samples were collected. The locations of these stations are

[2] Vertical and horizontal fractures were also filled by basaltic magma to form the dikes and sills. Although the sills and dikes represent pores through which geologic fluids were transported, the porosity of interest in the present study is that which hosted the meteoric groundwater of the hydrothermal system, and the contribution of the dikes and sills to the porosity is not considered.

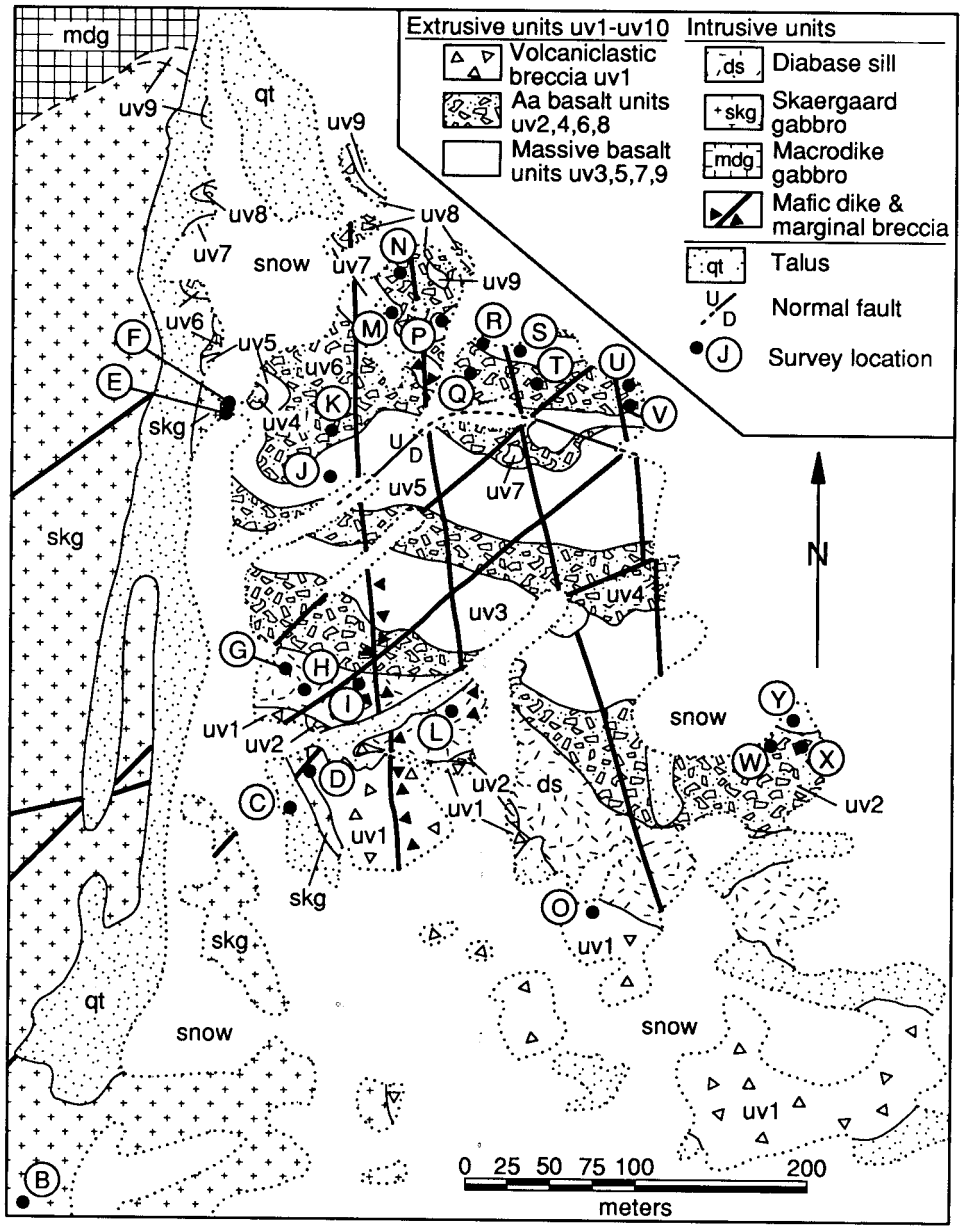

Fig. 10. Locations of survey stations B-Y. See figure 2 for stations A, Z, Ø, and Å.

TABLE 1

Summary of field survey stations and primary porosity

Survey†	Lithologic unit‡	Lithologic description	Survey area (m^2)	Meters from contact§	Mineral zone#	Φ^* (%)††
A	*skg*	coarse-grained gabbro	10.0	-400	-	0.0
B	*skg*	coarse-grained gabbro	1.5	-225	-	0.0
C	*skg*	fine-grained, grano-blastic-polygonal, marginal gabbro	1.0	-1	-	0.0
D	*uv1*	polymict breccia	5.0	1.5	olivine	0.0
E	*uv6*	monomict breccia	4.0	3	olivine	20.1
F	*uv5*	massive basalt flow	3.0	6	olivine	2.5
G	*ds*	medium-grained sill	9.6	30	pyroxene	0.0
H	*ds*	medium-grained sill	4.0	38	pyroxene	0.0
I	*ds*	medium-grained sill	16.0	50	pyroxene	0.0
J	*uv5*	massive basalt flow	4.0	54	pyroxene	0.6
K	*uv6*	monomict breccia	4.0	60	pyroxene	11.2
L	*ds*	medium-grained sill	4.0	103	pyroxene	0.0
M	*uv7*	massive basalt flow	6.0	112	pyroxene	1.7
N	*uv8*	monomict breccia; clast interspace completely filled by fine-grained basaltic detritus	24.0	131	pyroxene	1.8
O	*uv1*	polymict breccia	4.0	137	pyroxene	7.0
P	*uv9*	massive basalt flow	10.0	142	pyroxene	6.4
Q	*uv8*	vesicular, unbrecciated center of monomict breccia unit	4.0	155	pyroxene	9.0
R	*uv9*	massive basalt flow	4.0	165	pyroxene	3.0
S	*uv9*	massive basalt flow	2.5	180	pyroxene	4.9
T	*uv8*	vesicular, unbrecciated center of monomict breccia unit	4.0	190	pyroxene	4.6
U	*uv8*	monomict breccia	4.0	230	act + chl	22.0
V	*uv8*	monomict breccia	4.0	240	act + chl	14.9
W	*uv2*	monomict breccia	4.0	275	act + chl	4.9
X	*uv2*	monomict breccia	4.0	278	act + chl	4.9
Y	*uv3*	massive basalt flow	4.0	278	act + chl	2.6
Z	*lv*	massive basalt flow	25.9	1600	act + chl	2.6
Ø	*uv1*	polymict breccia	16.4	1600	act + chl	2.0
Å	*lv*	massive basalt flow	45.0	1900	act + chl	10.5

†See figures 2 and 10 for survey locations.

‡Unit abbreviations and locations given in figure 4. Undifferentiated lower Vandfaldsdalen flow units are abbreviated *lv*.

§Shortest distance to exposed or inferred contact corrected for later faulting and measured from center of survey area. Negative distances are west of the contact (gabbros) and positive distances are east of the contact (basalts and sill).

#Act + chl designates the *actinolite + chlorite zone*.

††Calculated using eq 2.

shown in figures 2 and 10 and the area, lithology, and metamorphic zone of each station are given in table 1.

Primary Pores

Primary pores include vesicles, vugs, and interstitial regions between fragments in aa flows and flow tops (fig. 5). In the massive flow units subspherical vesicles and larger, more irregular vugs constitute the primary void space. These features range from 0.1 to tens of centimeters in the longest dimension. Where not filled by basaltic detritus, interspace between breccia clasts in aa lavas defines irregularly shaped pores (fig. 5C). In aa lavas, continuously connected paths can be traced along the pore space for several meters in most exposures. Macroscopic primary

pore space in the polymict breccia is found predominantly in vesicular clasts, as the interspace between clasts in this unit is completely filled by fine-grained basaltic detritus.

Table 2 summarizes the mineral parageneses in primary pores throughout the study area. The similarity between parageneses in primary pores and those in metabasalt matrices in each mineral zone (fig. 7) and the common occurrence of subhedral forms of pore-filling crystals (fig. 5C) suggest that much primary pore space remained open at the time of Skaergaard emplacement and that this porosity was filled during prograde metamorphism of the basalts.

Measured values of Φ^* of primary pores for each survey station are given in table 1. Although the distribution of primary pores within and between units varies widely (fig. 11), average primary Φ^* is lowest in the Skaergaard gabbros and the sill (0.0 percent), intermediate in the massive flows (4.0 percent) and polymict breccia (7.0 percent), and highest in the monomict breccias (11.1 percent). In massive flows the highest values of primary Φ^* are found at flow tops. Maximum values of primary Φ^* in monomict flow breccias with nonvesicular centers occur at the bases and

TABLE 2

Mineral paragenesis in primary pores, horizontal veins, net veins, and hydrothermal breccias

	Metamorphic zone		
	Olivine & pyroxene zones 0-150 m*	Actinolite + pyroxene zone 150-210 m*	Actinolite + chlorite zone 210-300 m*
Grandite garnet	(2)	(2)	(2)
Titanite	1	1,2	1
Epidote		2	1,2
Clinopyroxene	1	1	2
Orthopyroxene	1	1	
Wollastonite	(1,2)		
Actinolite	2	2	1
Biotite	1	1	
Chlorite	2	2	1
Prehnite	2	2	1,2
Plagioclase	1	1	
K-feldspar	(1)	(1)	2
Quartz	(1)	(1)	1
Apophyllite	(3)		
Apatite	1	1	2
Ilmenite	1	1	
Cu-Fe sulfide	1,2	1,2	1,2
Fluorite	(2)		
Calcite	3	3	3

*(1) earliest minerals in pores; (2) intermediate minerals in pores; (3) latest minerals in pores. Parentheses denote rare occurrences, and blank entries indicate mineral not found in the metamorphic zone.

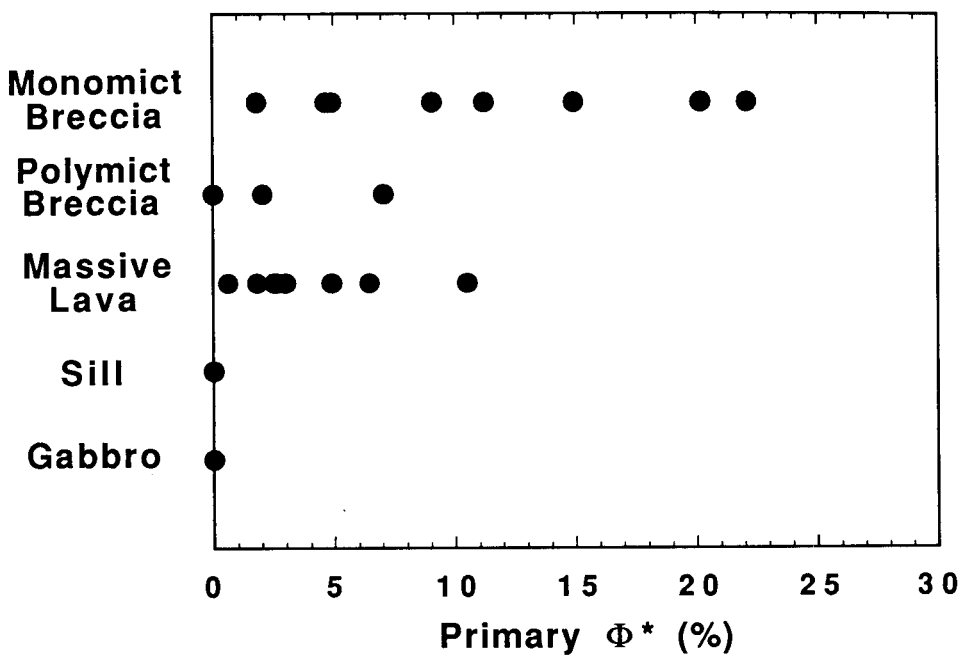

Fig. 11. Comparison of primary Φ* in the different lithologic units of the study area.

tops of the units. The distribution of pores within flows and variations in Φ* of primary pores between flows indicate that this parameter was stratigraphically controlled, forming bedding-parallel of high primary Φ* zones in the stratigraphy.

Horizontal Veins, Net Veins, and Hydrothermal Breccias

These pore types occur only in the basalts and are mutually contiguous locally. Horizontal veins are defined as veins with dips $< 30°$ from the horizontal. Net veins are groups of veins in which > 10 to 20 percent of the segments dip at angles $> 30°$ from the horizontal. Hydrothermal breccia is distinguished from horizontal and net veins by rotation and local transport of clasts. Two lines of evidence suggest that, like primary pores, these pores were filled during prograde metamorphism: (1) the earliest minerals filling these pore types are the same as those that fill primary pores (table 2), and (2) these minerals commonly have subhedral forms (fig. 12A). *Actinolite + chlorite zone* minerals are common in all three pore types as paragenetically late phases. Measured densities, orientations, and Φ* of horizontal veins, net veins, and hydrothermal breccias are summarized in table 3.

Horizontal veins.—Horizontal veins occur between 140 and 400 m from the contact and have variable densities. They define discontinuous, anastomosing, bedding-parallel planes that interconnect isolated, pri-

mary pores (fig. 12B). Horizontal veins were found in two-thirds of the surveys between 140 and 400 m from the contact. In the *actinolite + chlorite zone* (>210 m from the contact), these veins are easily identified in the field based on wide (~1 mm) alteration halos, but in thin section no identifiable fractures can be found. Instead, these structures are linear zones in which the modal abundance of *actinolite + chlorite-zone* minerals is greater than in the surrounding rock matrix. It thus appears that the horizontal veins >210 m from the contact represent submicroscopic cracks or zones of enhanced porosity along grain boundaries. In contrast, horizontal veins in the *pyroxene zone* between 140 and 210 m are distinct, mineral-filled fractures with sharp margins and apertures of ~0.1 mm. Densities of horizontal veins range up to 0.28 cm^{-1} (table 3). Values of Φ^* could only be determined for those horizontal veins with measurable apertures (table 3); these values range up to 0.003 percent.

Net veins.—These veins are restricted to the *pyroxene* and *olivine zones* <155 m from the contact and, like horizontal veins, do not occur in all surveys studied (table 3). The term "net vein" is used because, where this pore type is abundant, the wide range in orientations produces a net-like texture in outcrop. The vertical segments in net-vein occurrences have random strikes except in and near north-south dikes, where they parallel the dikes (fig. 12C). Net veins are distinguished from other vertical vein types described below by: (1) abrupt changes in dip of individual segments, and (2) the range in dips from horizontal to vertical (fig. 12C). Net veins in all samples represent open fractures now filled by secondary minerals and are continuous for centimeters to meters. Net veins have densities of up to 1.33 cm^{-1}. In addition, widths of individual vein segments range from 0.1 mm wide at 150 m to up to 3.5 mm wide near the contact, and, where net veins occur, they have higher Φ^* (0.004–0.229 percent) than localities crosscut by horizontal veins (0.001–0.003 percent; table 3).

Hydrothermal breccias.—Two north-south-trending, vertical breccia zones occur in the study area (figs. 4 and 12D). Both are located along the margins of north-south-trending dikes and are ~50 cm wide. The breccias are clast supported, with polymict fragments up to 10 cm in the longest dimension (fig. 12D), and the interspace between clasts is filled entirely by secondary minerals. Because these features crosscut the stratigraphy at high angles and the interspace between clasts is filled by secondary, hydrothermal minerals, they are referred to here as hydrothermal breccias, a descriptive term not intended to imply an origin by hydrothermal processes. The occurrence of different clast lithologies indicates fragment transport at least on a local scale. Values of Φ^* for hydrothermal breccias, measured on four slabbed hand specimens, are large and have a limited range of 11.2 to 12.7 percent (table 3).

Vertical Veins

Five mineralogically distinct types of vertical veins occur in the study area: pyroxene + oxide veins, calcic amphibole veins, quartz + feldspar

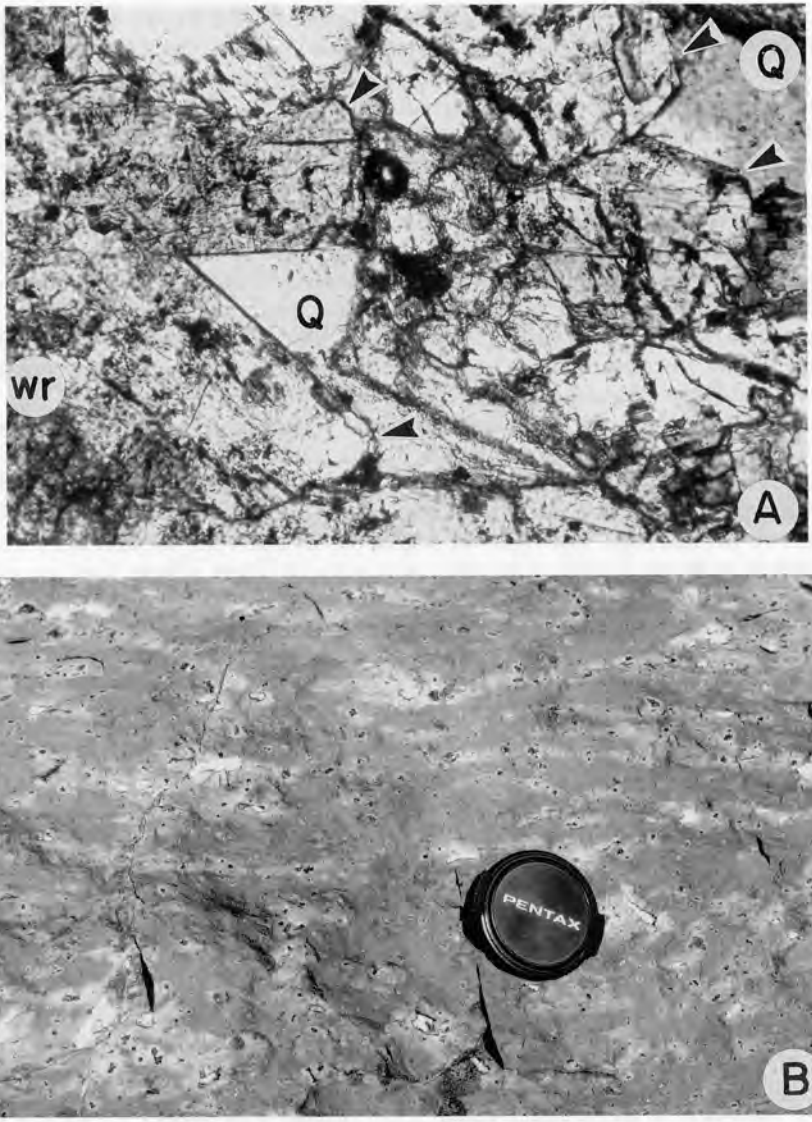

Fig. 12(A) Photomicrograph of secondary, tabular clinopyroxenes with subhedral terminations (shown with arrows) in a net vein 30 m from the contact. The vein margin and relatively fine-grained wall rock (wr) can be seen in the lower left corner. Residual pore space in this vein is filled by later quartz (Q). Nicols partly crossed. Field of view is 1 mm across. (B) Horizontal veins 220 m from the contact. Lens cap is ~5 cm in diameter. (C) Net veins in north-south dike 40 m from the contact. Note the predominantly vertical orientations, with sharp subvertical splays and occasional horizontal vein segments. Lens cap is 5 cm in diameter. (D) Polymict hydrothermal breccia at eastern margin of north-south trending dike (d) 42 m from the contact. The hydrothermal breccia can be traced into net veins within the dike. Pencil is 13 cm long.

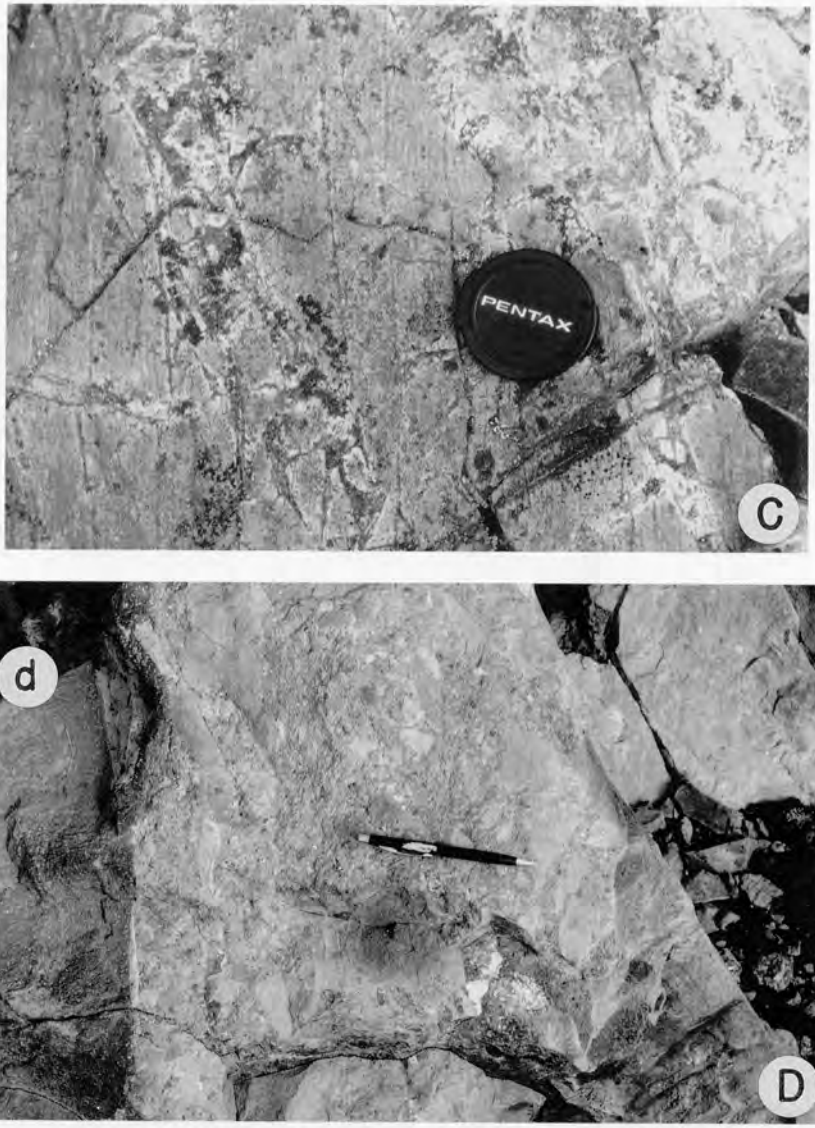

Fig. 12 (continued)

veins, quartz + epidote veins, and quartz veins. These veins are identical to those identified in the Skaergaard intrusion and other gabbros in the East Greenland Tertiary province by Bird, Rogers, and Manning (1986), and Bird, Manning, and Rose (1988), and the terminology used in those

TABLE 3

Horizontal veins, net veins, and hydrothermal breccias

Survey or sample	Lithologic unit	Meters from contact	Pore type†	Density (cm^{-1})	Segments >30° from horizontal (%)	Aperture (cm)	Φ^*(%)‡
A	*skg*	-400					0
B	*skg*	-225					0
C	*skg*	-1					0
D	*uv1*	1.5					0
E	*uv6*	3					0
F	*uv5*	6					0
G	*ds*	30	nv	0.653	97	0.35	0.229
H	*ds*	38					0
1361-1	*uv1*	38	hbx				12.3
1361-2	*uv1*	38	hbx				12.8
I	*ds*	50					0
J	*uv5*	54	nv	0.771	55	0.01	0.008
K	*uv6*	60					0
1359	*uv2*	73	hbx				11.2
L	*ds*	103					0
M	*uv7*	112					0
1330	*uv6*	120	hbx				12.7
N	*uv8*	131	nv	0.198	19	0.02	0.004
O	*uv1*	137					0
P	*uv9*	142	hv	0.282	0	0.01	0.003
Q	*uv8*	155	nv	1.327	23	0.01	0.013
R	*uv9*	165	hv	0.119	0	0.01	0.001
S	*uv9*	180	hv	0.101	0	0.01	0.001
T	*uv8*	190	hv	0.160	0	0.01	0.002
U	*uv8*	230	hv	0.268	0	?	?
V	*uv8*	240					0
W	*uv2*	275					0
X	*uv2*	278					0
Y	*uv3*	278	hv	0.782	0	?	?
Z	*lv*	1600					0
Ø	*uv1*	1600					0
Å	*lv*	1900					0

†Abbreviations: hv, horizontal veins; nv, net veins; hbx, hydrothermal breccia. Blank entries indicate that pores of these types were not found at the survey locality.

‡Horizontal and net vein Φ^* calculated using eq 3. Because their complex textures make field measurements difficult, Φ^* for horizontal and net veins was determined from sawed surfaces of oriented samples by dividing the lengths of vein segments by the planimetrically measured area of the slabbed surface. Hydrothermal breccia Φ^* calculated using eq 2.

studies is adopted here. Table 4 presents measured densities of each vertical vein type. The strikes of vertical veins in the 28 surveys are given as rose diagrams in figure 13 and summarized for each vertical vein type in figure 14.

Pyroxene + oxide veins.—Pyroxene + oxide veins (fig. 15A) weather rusty red or brown and are discontinuous (< 10 m long, usually < 1 m long) with irregular walls. These veins occur in both *pyroxene zone,* where mean widths are 0.1 to 1 mm, and in the *olivine zone,* where apertures commonly exceed 1 mm. Their rust-colored weathering makes them

TABLE 4

Vertical vein densities

Survey	Lithologic unit	Meters from contact[c]	Density (cm^{-1}) by vein type*					
			Pyroxene + oxide	Calcic amphibole	Quartz + feldspar	Quartz + epidote	Quartz	Total
A	*skg*	-400		0.006				0.006
B	*skg*	-225		0.214				0.214
C	*skg*	-1		1.542				1.542
D	*uv1*	1.5	0.021	0.283				0.304
E	*uv6*	3	0.034	0.096				0.130
F	*uv5*	6		0.121				0.121
G	*ds*	30	0.012	0.042	0.003			0.057
H	*ds*	38	0.023	0.160	0.015			0.198
I	*ds*	50	0.002	0.015	0.026			0.043
J	*uv5*	54	0.009	0.254				0.263
K	*uv6*	60	0.025	0.071				0.096
L	*ds*	103	0.012	0.167	0.024			0.203
M	*uv7*	112	0.016	0.127				0.143
N	*uv8*	131	0.004	0.217				0.221
O	*uv1*	137	0.009	0.047				0.056
P	*uv9*	142	0.002	0.029				0.031
Q	*uv8*	155	0.025	0.156				0.181
R	*uv9*	165	0.030	0.133				0.163
S	*uv9*	180		0.109				0.109
T	*uv8*	190	0.030	0.114				0.144
U	*uv8*	230	0.005	0.032				0.037
V	*uv8*	240		0.059			0.085	0.144
W	*uv2*	275				0.048		0.048
X	*uv2*	278				0.074		0.074
Y	*uv3*	278				0.142		0.142
Z	*lv*	1600				0.024		0.024
Ø	*uv1*	1600				0.019		0.019
Å	*lv*	1900				0.015		0.015

*Blank entries indicate vein type not observed at the survey locality.

indistinguishable from rust-weathering calcic amphibole veins (see below) in the field; however, all N30W to N20E rust-colored veins examined petrographically were pyroxene + oxide veins, and all veins with these orientations were assumed to be of this type. The mineralogy of these veins includes clinopyroxene, orthopyroxene, ilmenite, and minor plagioclase, olivine, and magnetite. Unlike metabasalt matrices in which olivine is found only at <10 m from the contact, olivine occurs sporadically in pyroxene + oxide veins up to 50 m from the contact. Vein olivines are poikilitic and include fine-grained plagioclase, pyroxene, and ilmenite, similar to olivine porphyroblasts in the hornfels. In addition, vein-filling minerals and contacts with wall-rock minerals have granoblastic-polygonal textures (fig. 15A). These textures suggest that pyroxene + oxide veins were metamorphosed during prograde development of the host hornfels. Pyroxene + oxide veins have low densities (<0.034 cm^{-1}; table 4) and, assuming initial apertures of 0.1–1 mm, low Φ^* of 3×10^{-3} to 3×10^{-4}.

Calcic amphibole veins.—Bird, Manning, and Rose (1988) differentiated five types of calcic amphibole veins in the East Greenland gabbros.

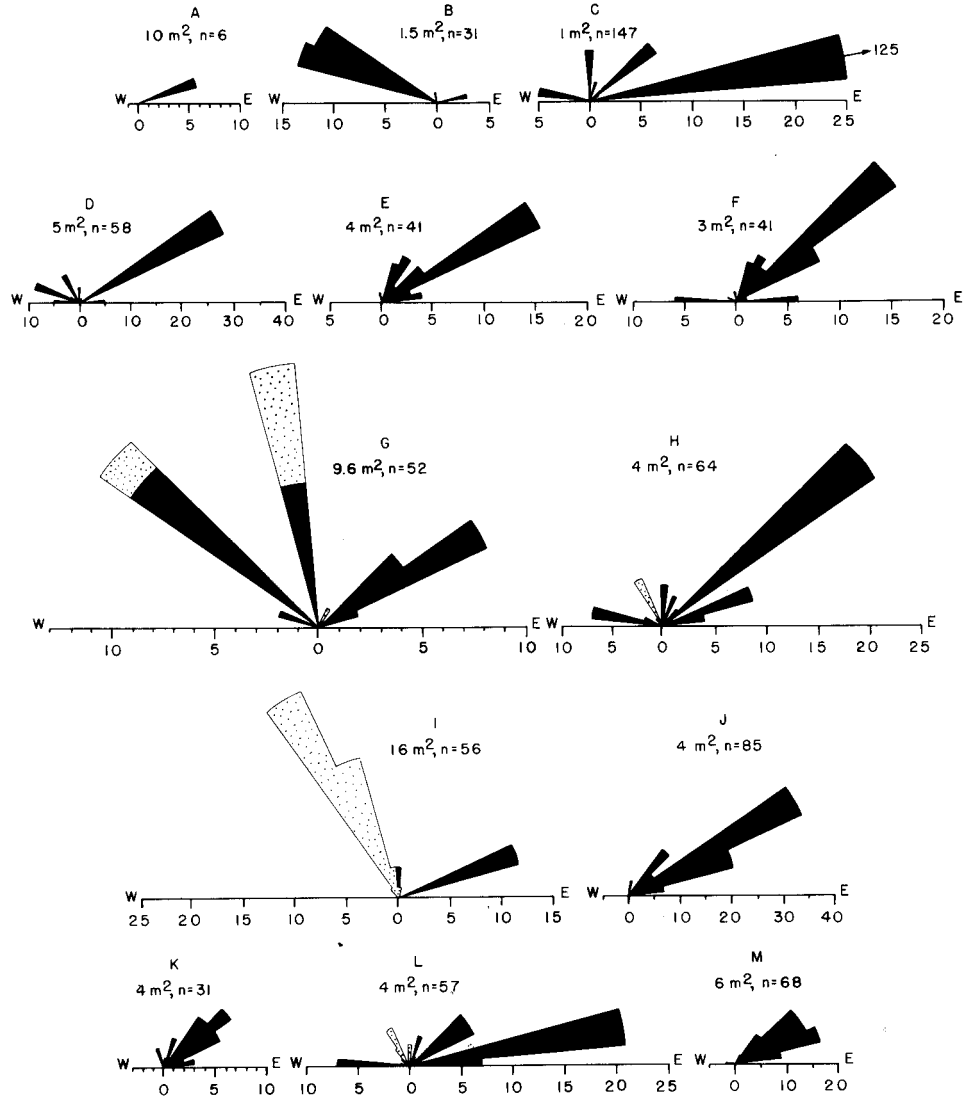

Fig. 13. Rose diagrams showing abundance and strikes of vertical veins. Survey stations are labelled with letters (A-Z, Ø, Å) whose locations are shown in figures 2 and 10. The area of each survey (in square meters) and the number of measurements (n) are also given above each diagram. All diagrams are oriented with north to the top, and the units of the horizontal axes are the number of observations. Vein types include calcic amphibole and pyroxene + oxide veins (filled pattern), quartz + feldspar veins (stippled), epidote + quartz veins (unfilled), and quartz veins (hachured).

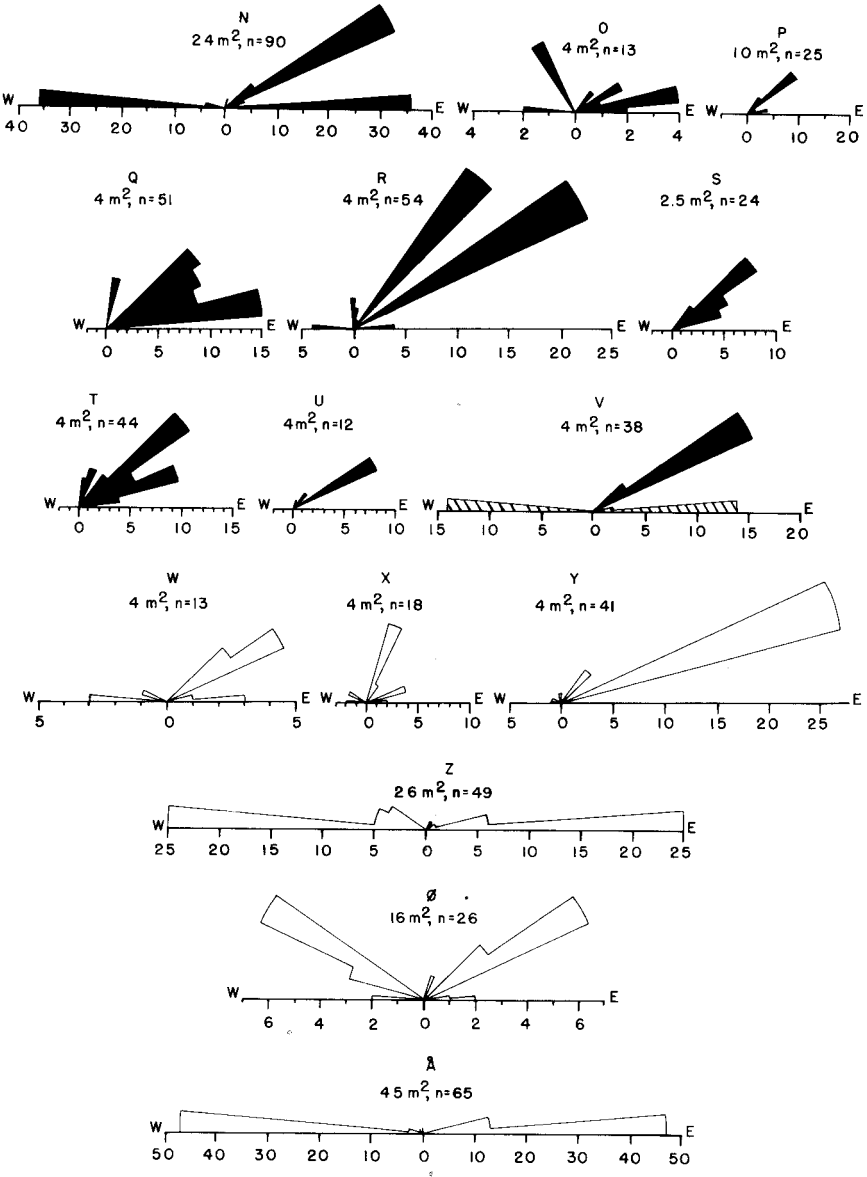

Fig. 13 (continued)

Three of these types occur in the study area: calcic amphibole + pyroxene, calcic amphibole + epidote + albite, and actinolite + chlorite. Calcic amphibole veins are continuous for tens of meters, are ≤ 3 mm wide, and weather black, rusty red, or brown. For details of mineral textures and

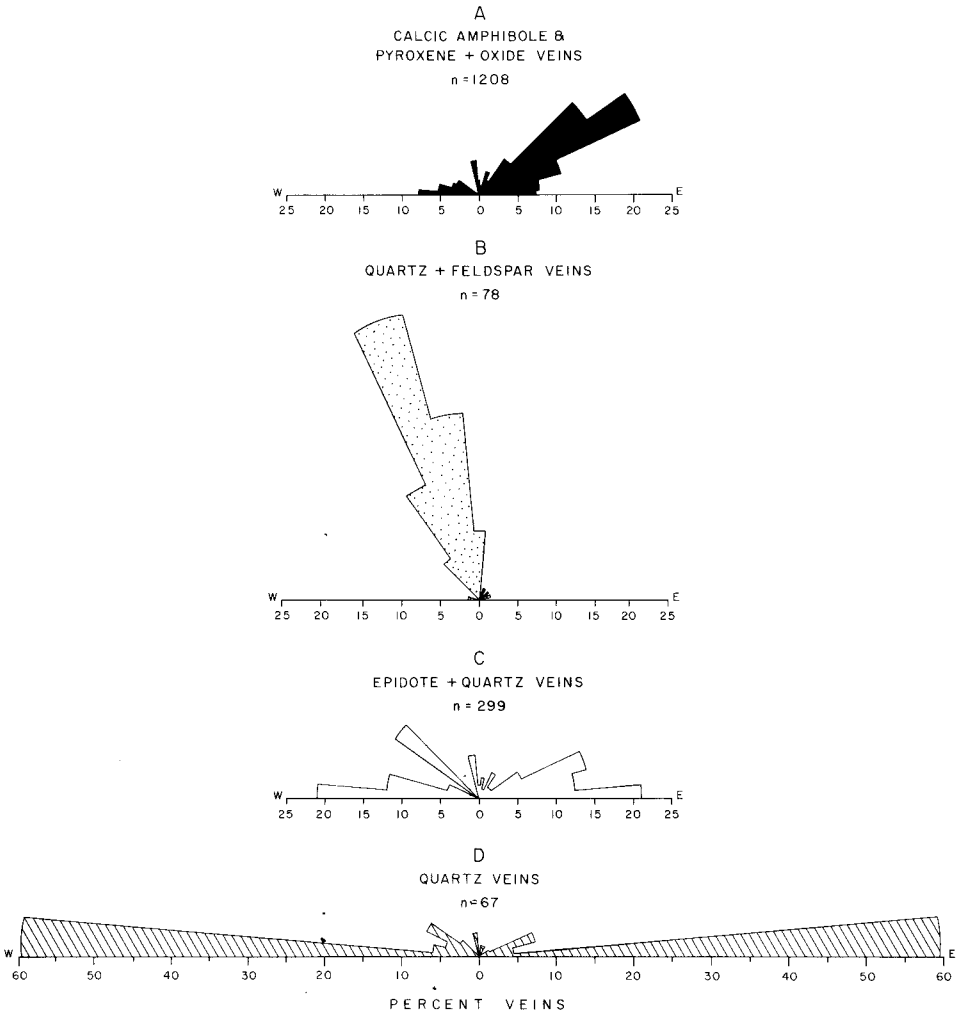

Fig. 14. Rose diagrams summarizing strikes and abundance of each vertical vein type (in percent). Measurements include those at the survey stations and individual observations throughout the study area. Diagrams are oriented east-west with north to the top, and the number of observations (n) is given for each vein type: (A) calcic amphibole and pyroxene oxide veins; (B) quartz + feldspar veins; (C) epidote + quartz veins; and (D) quartz veins. The mode at N20W in (B) is 38 percent of quartz + feldspar vein orientations.

compositions see Bird, Rogers, and Manning (1986), Manning and Bird (1986), Rogers and Bird (1987), and Bird, Manning, and Rose (1988).

Calcic amphibole + pyroxene veins are found only in the Marginal Border Group gabbros. They weather black and are up to 0.5 mm wide. Two orientations occur in the study area: east-west ±20° and N20W. The

veins are filled with brown hornblende (fig. 15B) overgrown by blue-green hornblende, actinolite, and chlorite. In the wall rock, plagioclase is altered to chlorite, and olivine to the assemblage talc + magnetite + actinolite ± cummingtonite up to 2 mm from vein margins. Magmatic augites are altered to hydrothermal clinopyroxenes as described by Manning and Bird (1986).

Calcic amphibole + epidote + albite veins are uncommon in East Greenland hydrothermal systems (Bird, Manning, and Rose, 1988), and only one such vein was found in the Marginal Border Group gabbros of the study area. This vein is ~0.5 mm wide, trends N70E, and is distinguished from calcic amphibole + pyroxene veins because, in addition to containing actinolite and hornblende as vein fill, it also contains chlorite, epidote, albite, and brecciated and rotated pieces of wall-rock plagioclase altered to albite. In the wall rock, augite is altered to hydrothermal clinopyroxene and actinolite, and plagioclase is altered to albite.

Actinolite + chlorite veins occur in the gabbros and the basalts up to 240 m from the contact and are the most abundant type of calcic amphibole vein, accounting for > 99 percent of all observed calcic amphibole veins in the study area. In outcrop (fig. 15C) actinolite + chlorite veins weather rusty brown and red and cannot be distinguished in the field from the pyroxene + oxide veins described above. These veins are filled by actinolite and chlorite ± cummingtonite and quartz and locally have alteration halos up to 1 cm wide (fig. 15D). Veins of this type are mineralogically similar to those described by Rogers and Bird (1987) near mafic dikes in the Skaergaard intrusion.

Calcic amphibole veins are ubiquitous, occurring in all surveys < 240 m from the contact, but densities of these veins range widely (table 4). Although apertures range from < 0.1 to 3 mm, most are ~0.1 mm, and calculated values of Φ^* range from 10^{-2} to 10^{-4} percent, with a mean of 6×10^{-3} percent.

Inspection of the individual survey data for calcic amphibole veins in figure 13 suggests that there are three general orientations in addition to the north-south maxima defined by the pyroxene + oxide veins: ~N50E, ~east-west, and ~N50E. Cumulative data presented in figure 14 show that northeast orientations are the most abundant (56 percent at N40–N70E), whereas east-west veins are moderately abundant, and northwest veins are relatively uncommon.

Quartz + feldspar veins.—Veins of this type occur within 125 m of the contact in the basalts, range in length from 1 to 30 m, and are usually ~1 cm wide, although several veins up to 30 cm wide were observed. Combining the vein densities given in table 4 with 1 cm apertures gives an average Φ^* of 1.7×10^{-2} percent. Quartz + feldspar veins also show wide range in morphology, from anastomosing, irregular segregations to veins with planar margins (fig. 16A). Trends of 95 percent of the quartz + feldspar veins are N20W ± 20° (fig. 14). Veins of this type are filled by quartz, locally with acicular actinolite inclusions, K-feldspar, and minor biotite and albite. Within ~30 m of the contact, quartz and K-feldspar in

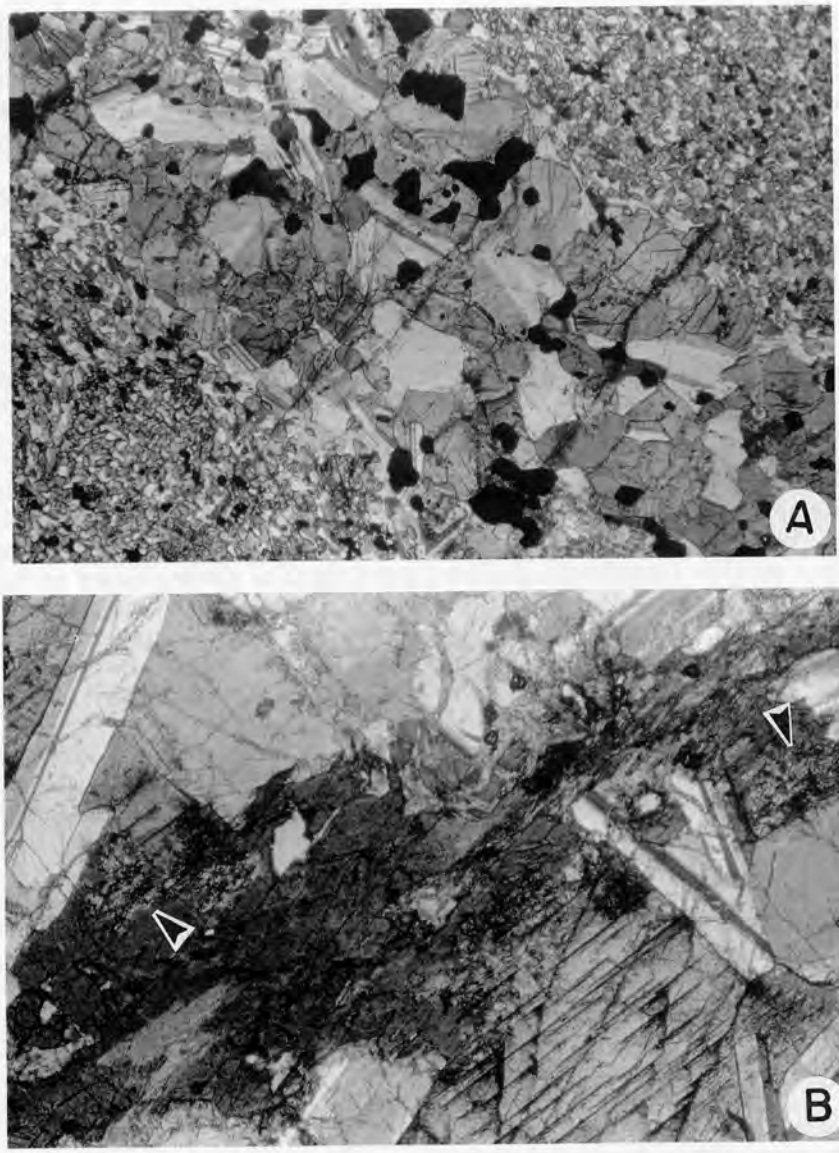

Fig. 15(A) Photomicrograph of pyroxene + oxide vein (bottom right to top left) 10 cm from contact. The vein also contains plagioclase. Note granoblastic polygonal textures of vein-filling minerals and vein-wall rock contact. Partly crossed nicols. Field of view is 6 mm wide. (B) Photomicrograph of hornblende + clinopyroxene vein (bottom left to top right) in coarse-grained Marginal Border Group gabbro. The vein is filled primarily by hornblende (dark phase, note distinct amphibole cleavage), magmatic augite is altered to hydrothermal clinopyroxene (arrows), and plagioclase appears unaltered optically. Nicols partly crossed. Field of view is 3 mm wide. (C) Photograph of actinolite + chlorite veins ~80 m from the contact. Lens cap is 5 cm in diameter. (D) Photomicrograph of actinolite + chlorite vein (bottom right to top left) in *pyroxene zone* hornfels. Plane light. Field of view is 6 mm wide.

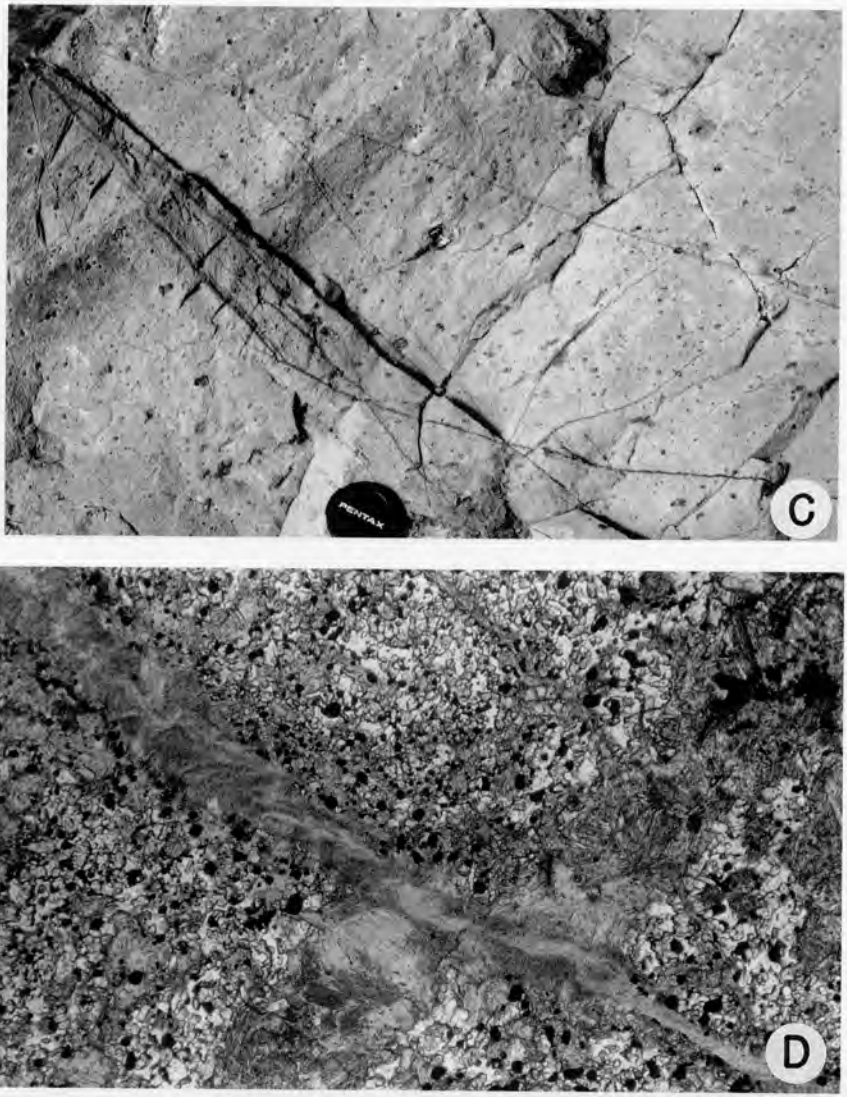

Fig. 15 (continued)

many of these veins are intergrown in granophyric textures (fig. 16B). We interpret these granophyres as having crystallized from a silicate liquid based on textural and mineralogic similarities to granophyres within the Skaergaard intrusion described by Wager and Brown (1967) and Hirschmann (1987, 1988). Like those in the Skaergaard, granophyres in the study area lack fine-grained chilled margins. Granophyric

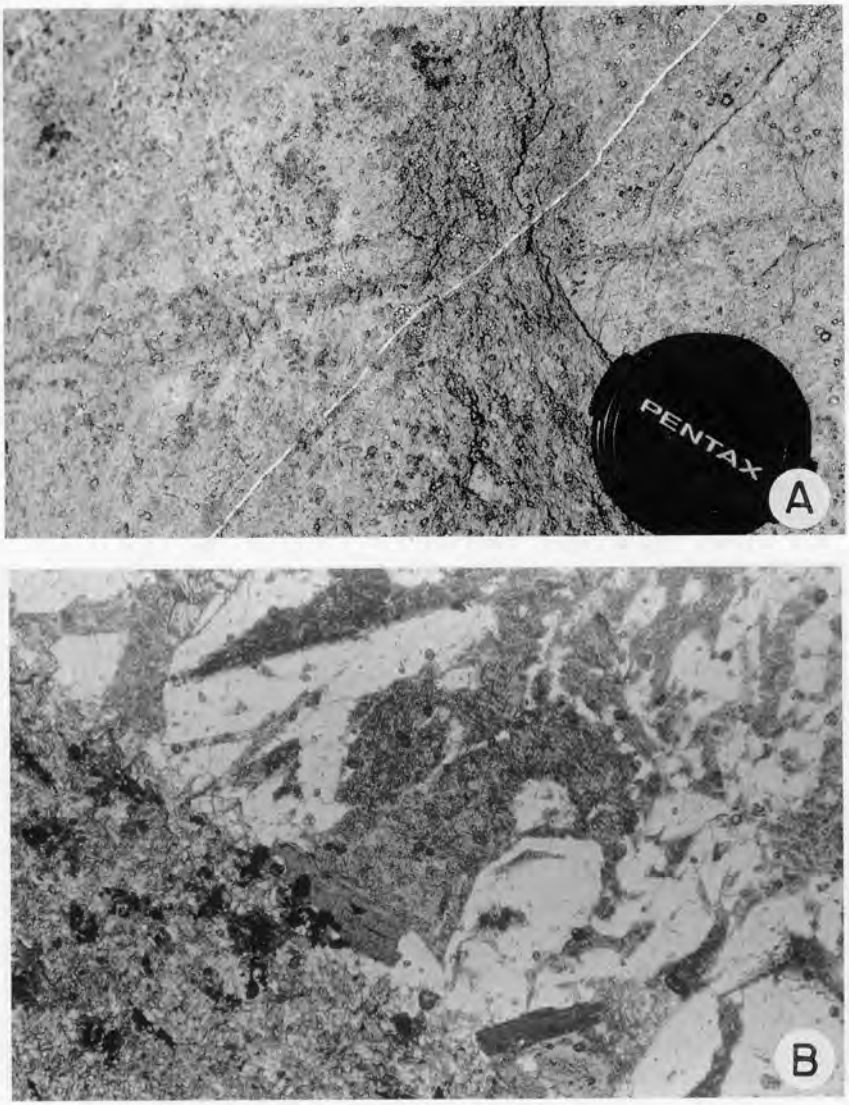

Fig. 16(A) Quartz + feldspar vein (white) crosscutting massive basalt 20 m from the contact. Lens cap is 5 cm in diameter. The quartz + feldspar vein is crosscut by an actinolite + chlorite vein (dark) in the center of the photograph. (B) Photomicrograph showing granophyric intergrowth of quartz and K-feldspar at the margin of a quartz + feldspar vein. Plane light. Field of view is 3 mm wide. (C) Epidote + quartz veins with ~1 cm alteration haloes in the pre-Skaergaard diabase sill 250 m east of the contact. (D) Photomicrograph of epidote + quartz vein. Vein is filled by epidote and minor quartz. Crossed nicols. Field of view is 3 mm wide.

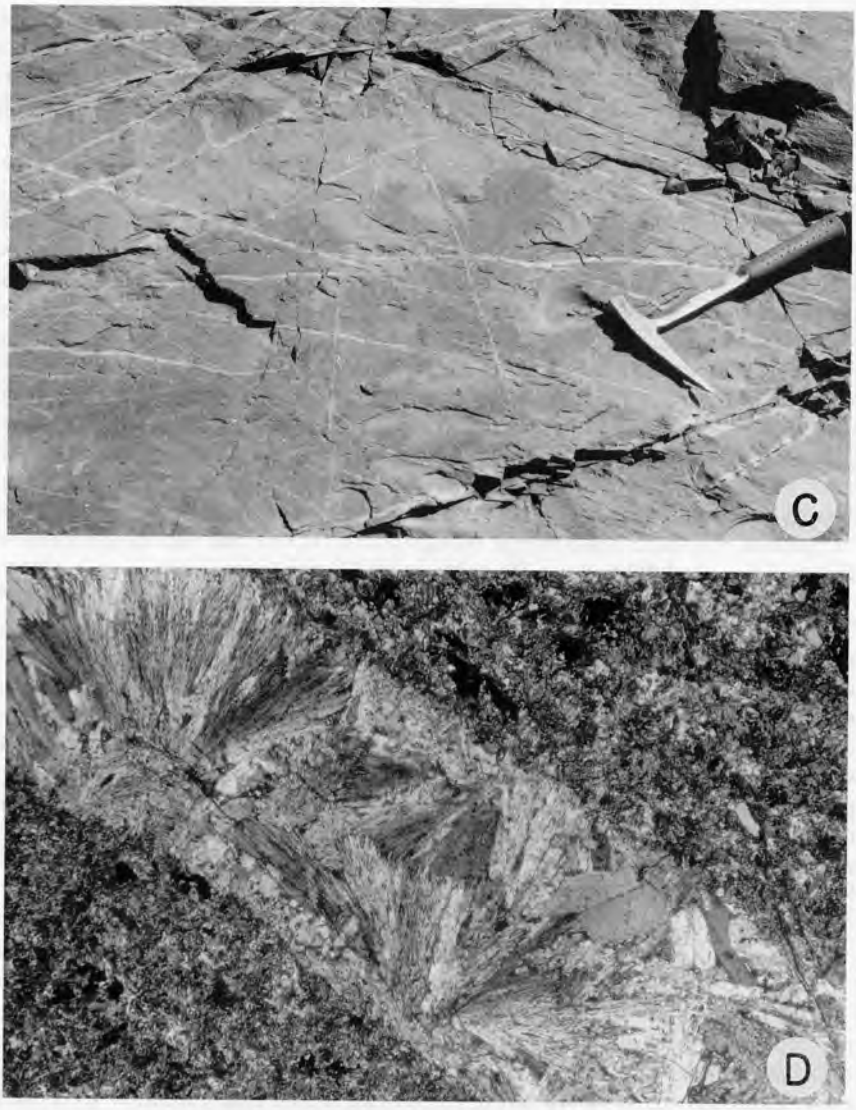

Fig. 16 (continued)

intergrowths were not observed beyond ~30 m from the contact, and the quartz + feldspar assemblages in these more distal structures probably precipitated from aqueous solutions evolved from or equilibrated with the granophyres. This interpretation is supported by the common occurrence of quartz + feldspar veins 30 to 125 m from the contact with drusy cavities lined by subhedral minerals. Interaction of pore fluids with the

granophyres is also suggested by local, fluorine-rich alteration assemblages that overgrow prograde metamorphic minerals near the contact (Manning and Bird, 1987, 1990). Crystallization of quartz and feldspar assemblages from both aqueous solutions and silicate liquids may explain the contrasting morphologies but similar trends of these structures.

Epidote + quartz veins.—Epidote + quartz veins occur in the *actinolite + chlorite zone* of the study area and are found up to 15 km from the Skaergaard intrusion. These veins are typically 0.1 to 1 mm wide with alteration halos up to 1 cm wide (fig. 16C). Epidote + quartz veins are filled primarily by epidote and quartz (fig. 16D), although the modal abundance of either phase may range from ~5 to 95 percent in thin section and in outcrop. Minor titanite, grandite garnet, salitic clinopyroxene, chlorite, actinolite, calcite, and chalcopyrite may also occur in these veins. Small, drusy pockets in vein centers are partially filled by calcite. In the wall rock about these veins clinopyroxene is altered to actinolite, plagioclase to albite and K-feldspar, and ilmenite to titanite. Orientation maxima occur at east-west, northwest, northeast, and N10W (fig. 14). No offsets between these different vein orientations were observed. Densities of epidote + quartz veins range from 0.015 to 0.142 cm^{-1} in the *actinolite + chlorite zone,* and Φ^* ranges from 10^{-2} to 10^{-4} percent.

Quartz veins.—Monomineralic quartz veins trend east-west ± 20°. They are typically thin (0.1 mm wide) and discontinuous. Vertical slickensides are common on vein-wall surfaces. One thick (10 cm wide) quartz vein offsets bedding contacts by ~1 m. The veins locally display crack-seal textures (Ramsey, 1980), with fragments of wall rock included in the vein quartz. As they crosscut all other vein types, they were the latest veins to form in the study area. Although individual quartz veins occur throughout the study area, their low abundance is illustrated by the fact that they were observed in only one survey (*V*, fig. 14), where they occur as a swarm with 1 mm apertures. Quartz veins at this locality have Φ^* of 9×10^{-3} percent.

PORE EVOLUTION AND STRUCTURAL HISTORY

Origin and Relative Age of Pore Types

Pore types were distinguished in the previous section on the basis of morphology and mineral fill. These pore types can be divided into six relative-age groups using crosscutting relations and mineral parageneses. Each group is designated P_n, where n increases from 0 to 5 with increasing age after extrusion of the lavas.

P_0: primary pores.—Primary pores formed during extrusion and crystallization of the lavas and were therefore the first pore types. During burial the primary pore space was partly filled by low-temperature minerals such as zeolites similar to those found in the Tertiary basalts exposed to the north (Larsen and Watt, 1985). Vertical, east-west-trending, tholeiitic dikes crosscut the lower basalts near the coast (fig. 1). These dikes were emplaced during burial of the volcanic pile and were feeders to the Plateau Basalts that overlie the basalts of the study area (fig.

1; Nielson, 1978). Delaney and others (1986) suggest that dike orientations in rift environments are good indicators of principal stress orientations at the time of dike emplacement. The attitudes of the early east-west dikes thus indicate that regional, least-compressive stress (σ_{min}) was approximately north-south and horizontal at this time.

P_1: north-south vertical veins.—North-south-trending vertical veins include pyroxene + oxide veins in the *pyroxene* and *olivine zones* and epidote + quartz veins in the *actinolite + chlorite zone*. Maximum densities of north-south-trending veins decrease with increasing distance from the margins of north-south dikes (fig. 17), suggesting fracture formation during dike emplacement (Delaney and others, 1986; Rogers and Bird, 1987). As noted above, metamorphic mineral assemblages and granoblastic-polygonal textures in north-south dikes and veins (fig. 15A) indicate formation before Skaergaard emplacement. Because these veins are crosscut by all other types of secondary pores, they represent the oldest secondary porosity in the study area. No crosscutting relations were observed between early east-west dikes and the north-south dikes (fig. 4); however, north-south-trending dikes found elsewhere in the region are part of a later set that was structurally, petrologically, and geochemically

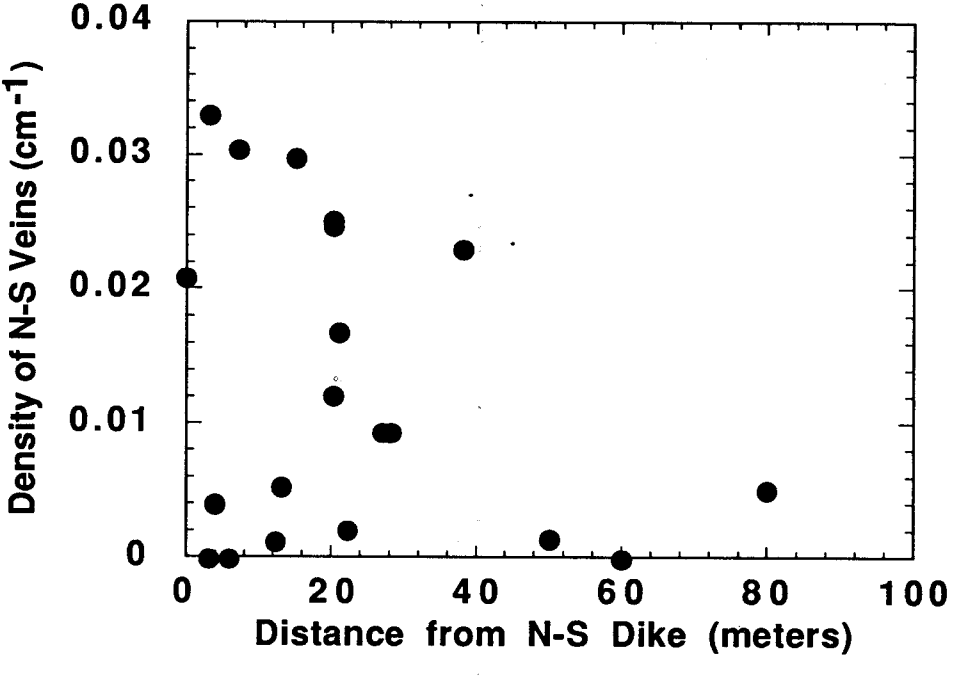

Fig. 17. Density of north-south-trending veins as a function of distance from north-south dikes in the study area.

related to the Skaergaard intrusion (Brooks and Nielsen, 1978; Nielsen, 1978). The horizontal, east-west σ_{min} implied by vertical north-south dikes and P_1 veins thus signify a local departure from the regional horizontal north-south orientation of σ_{min} just prior to Skaergaard emplacement.

P_2: horizontal veins, net veins, and hydrothermal breccias.—The relative age of these pores is constrained by three observations: (1) the three pore types are mutually contiguous, suggesting coeval formation; (2) net veins occur in north-south dikes (fig. 12C) and therefore postdate P_1; and (3) all three pore types are crosscut by the pore types described below. As noted above, the textures and phase relations of minerals filling P_2 require formation during prograde recrystallization of the basalts. This would have occurred as temperatures increased in the host basalts after inflation of the Skaergaard magma chamber until peak temperatures were attained at ~40,000 yrs after emplacement (fig. 8).

Fluids in pores would have expanded as temperatures increased in the aureole during prograde metamorphism, and P_2 structures probably represent deformation caused by these expanding fluids. The change in fluid pressure in an isolated pore with increasing temperature at constant volume can be expressed as

$$\left(\frac{\partial P}{\partial T}\right)_V = \frac{\alpha}{\beta}, \tag{4}$$

where α and β are the coefficients of isobaric thermal expansion and isothermal compressibility of H_2O. Figure 18 shows the temperature dependence of α/β at 1 kb, the approximate lithostatic pressure in the study area at the time of magma emplacement. It can be seen that the partial derivative represented by eq 4 is always positive, with a maximum at ~200°C. The positive sign of α/β means that pore pressures would have continually increased as temperatures rose in the volcanics after emplacement of the Skaergaard magma. If these fluid pressures exceeded σ_{min} and rock strength, fracturing would have resulted (Knapp and Knight, 1977; Knapp and Norton, 1981; Norton, 1984). Two observations support this origin for P_2. First, horizontal veins define segments linking primary pores such as vesicles (fig. 12B). And second, as shown in figure 19, P_2 structures formed preferentially in massive lithologies with low primary porosity, where isolated primary pores were more abundant (compare fig. 5A and B). The lower densities of horizontal and net veins in rocks with high primary Φ^* suggest that the porosity in these lithologies had a higher degree of connectivity and that thermal expansion of pore fluids led to fluid flow.

The proposed origin of P_2 structures can thus be summarized as follows. The thermal pulse that rapidly migrated into the basalts shortly after magma emplacement caused brittle deformation as pore fluids expanded, and this deformation front also migrated out into the basalts. The horizontal veins are the most distal P_2 structures, occurring from 140 to 400 m, and thus record the furthest migration of this deformation

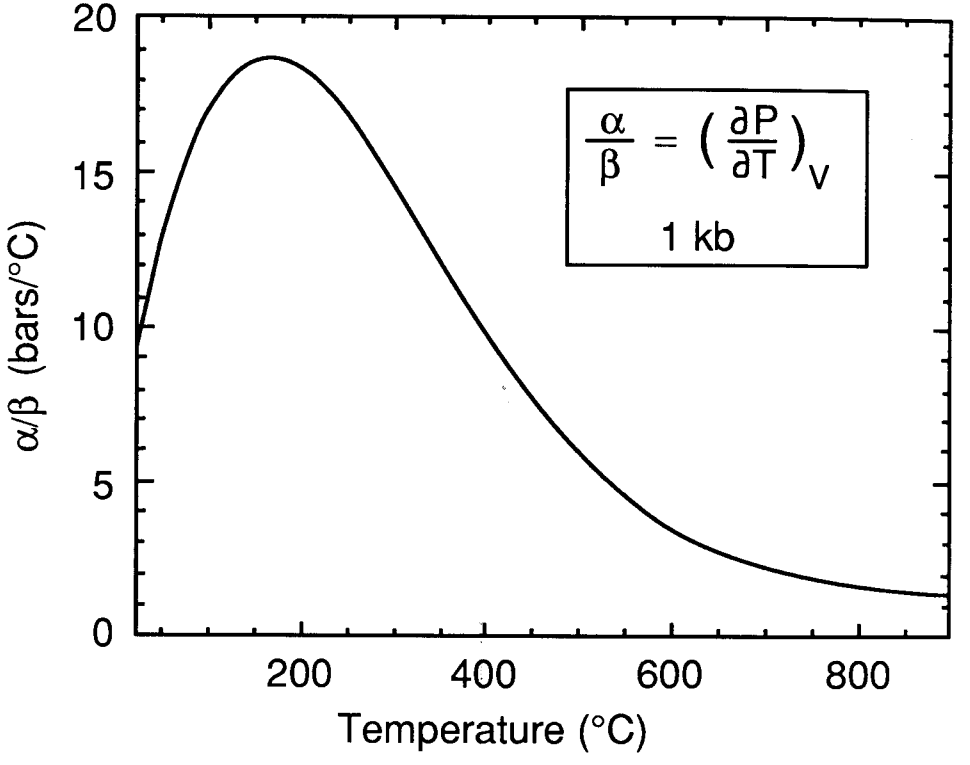

Fig. 18. The ratio of coefficients of isobaric thermal expansion (α) to compressibility (β) for H_2O as a function of temperature at 1 kb calculated from equations and data of Helgeson and Kirkham (1974).

front. These horizontal vein orientations indicate vertical σ_{min} and suggest that magma pressures exerted on the walls of the intrusion exceeded vertical pressures due to overburden. Within 155 m of the contact P_2 structures change from horizontal to net veins. The occurrence of net veins with disparate strikes and vein-segment dips ranging from horizontal to vertical suggests that the stress regime closer to the contact was nearly isotropic, such that slight, local, lithologic, or mineralogic heterogeneities allowed fracture propagation in a variety of directions with abrupt changes in orientation. The change from horizontal- to net-vein textures can be seen in figure 20, which shows that the percentage of P_2 segments with dips $> 30°$ from the horizontal increases as the intrusion is approached. In addition, net veins have higher Φ^* than horizontal veins (table 3). The higher P_2 strains recorded near the contact are probably due to the higher temperatures attained within 155 m ($> 780°C$, Manning, ms), which could have led to multiple fracturing episodes as pore fluid pressures repeatedly built up, exceeded the rock's tensile strength,

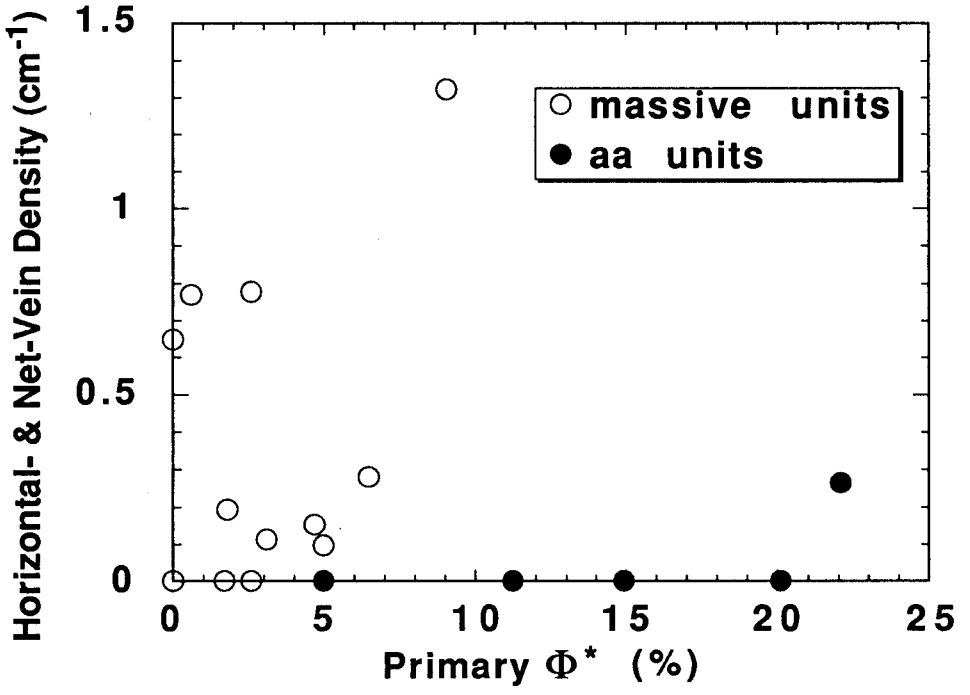

Fig. 19. Measured horizontal- and net-vein densities as a function of primary Φ* in aa and massive units. Massive units include vesicular and intrusive lithologies, the massive, central portions of aa flows, and the aa flow at survey N in which breccia interspace is filled by fine-grained basaltic detritus (table 1).

and then were released by fracturing. The two hydrothermal breccia zones in this region also may have formed by pore fluid expansion (Delaney, 1982); however, the occurrence of the hydrothermal breccias near the margins of dikes may also be a consequence of earlier fracturing or brecciation of the host volcanics during dike emplacement and cooling as is described around dikes in the Colorado Plateau by Delaney and Pollard (1981) and Delaney and others (1986). The changing geometry of the pore network, the higher strains, and the presence of the hydrothermal breccias have important implications for fluid flow during P_2 time (see below).

P_3: quartz + feldspar and calcic amphibole + pyroxene veins.—In the basalts, quartz + feldspar veins crosscut P_2 structures and postdate hornfels development. However, because the granophyric quartz + feldspar veins do not have chilled margins, they must have been emplaced when the temperatures of the rocks of the *pyroxene* and *olivine zones* remained sufficiently high that the silicate liquid in the fractures did not cool rapidly. The N20W ± 20° orientation of 95 percent of the quartz +

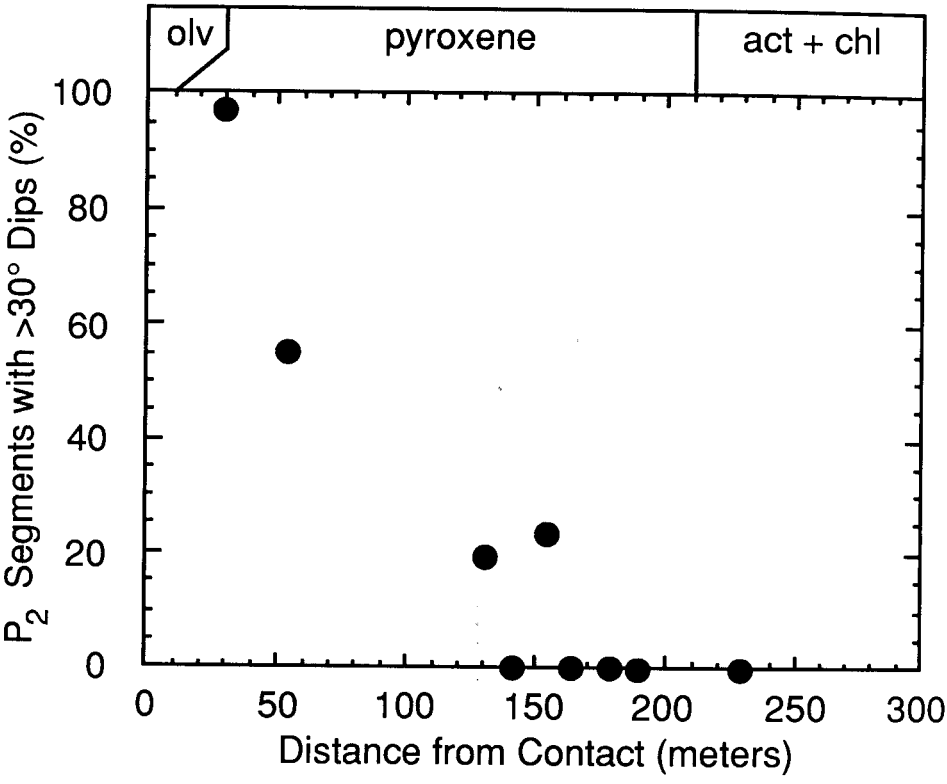

Fig. 20. Percent of horizontal and net vein segments (P_2) oriented >30° from the horizontal as a function of distance from the contact.

feldspar veins (fig. 14) is approximately parallel to that of the Skaergaard contact in the study area, implying horizontal σ_{min} normal to the walls of the intrusion (east-northeast-west-southwest). The stress regime, textures, and age relations associated with P_3 are consistent with formation during cooling and contraction of the Skaergaard gabbros shortly after magma solidifcation.

The earliest veins in the Skaergaard gabbros are calcic amphibole + pyroxene veins (Bird and and others, 1986, 1988). Near the east contact their orientations are ~east-west and ~north-south. These orientations are perpendicular and parallel to the contact at this locality, similar to early vein orientations near other contacts of the Skaergaard and probably represent the earliest fracturing due to contraction of the Marginal Border Group at temperatures of >600° to 900°C (Knapp and Norton, 1981; Bird, Manning, and Rose, 1988). Because quartz + feldspar veins in the basalts are also interpreted to have formed during gabbro contraction, these two vein types probably formed at the same time.

P_4: actinolite + chlorite and epidote + quartz veins.—Actinolite + chlorite veins crosscut quartz + feldspar veins (fig. 16A). No crosscutting relations between this pore type and epidote + quartz veins were observed; however, actinolite + chlorite and epidote + quartz veins have similar orientations (fig. 14) suggesting formation at the same time in different parts of the aureole. Epidote + quartz veins and actinolite + chlorite veins have orientation maxima of east-west, northeast, and northwest (figs. 13 and 14). East-west veins both crosscut and are crosscut by northeast veins, but no definitive crosscutting relations were observed between northwest veins and other P_4 veins. Figure 21 shows that, like the north-south veins, maximum observed densities of northeast veins decrease with increasing distance from northeast dikes, suggesting that these fractures formed during dike emplacement. The dominant northeast-trending feature in this area is the Vandfaldsdalen macrodike (figs. 1 and 4). The map area of figure 4 is the only locality in the Tertiary stratigraphy east of the Skaergaard in which we have observed a high density of northeast dikes and veins. These observations argue for a similar age for the macrodike, the smaller northeast dikes, and the northeast veins. Although no east-west or northwest dikes occur in the area of figure 4, these dike orientations occur throughout the region (fig.

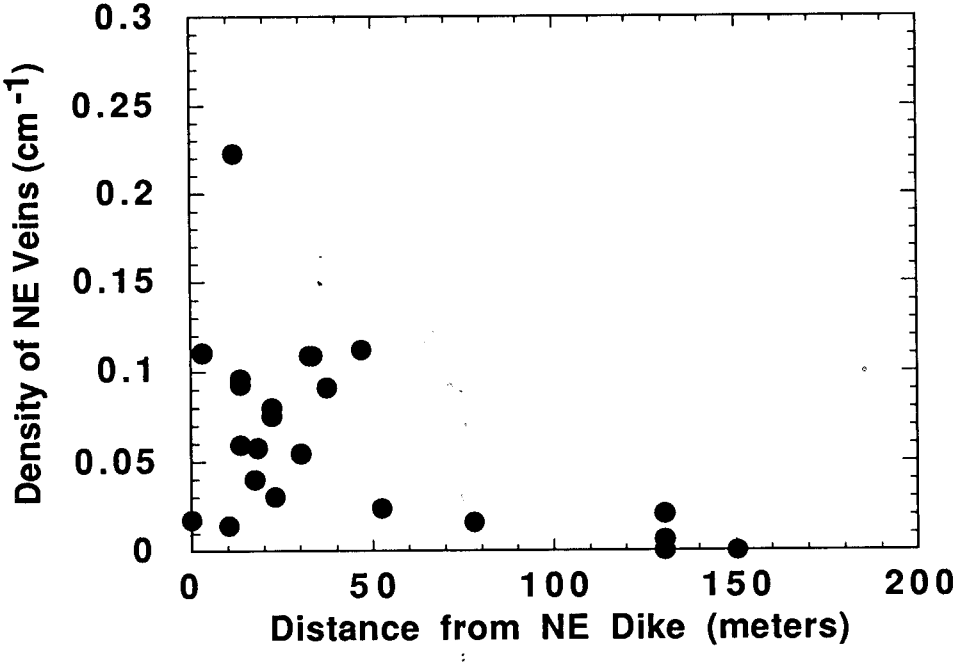

Fig. 21. Northeast actinolite + chlorite and epidote + quartz vein densities as a function of distance from northeast dikes in the study area.

6), and the formation of east-west and northwest actinolite + chlorite and epidote + quartz veins was probably related to the regional tectonic activity associated with the emplacement of dikes with these trends. The orientations of the most voluminous dikes (east-west ±20°; fig. 6) indicate horizontal, north-south σ_{min}. Local deviations in σ_{min} to north-northwest and northeast during this time are indicated respectively by the northeast-trending and the northwest-trending dikes and veins.

Actinolite + chlorite veins in the gabbros of the study area have orientation maxima at east-west, northeast, and northwest (surveys A–C, fig. 13). These veins postdate calcic amphibole + pyroxene veins in the gabbros and, based on similarities in orientation and mineral assemblage, are probably related to the P_4 veins in the basalts. No veins crosscut the single calcic amphibole + epidote + albite vein observed in the gabbros, but its N70E trend is consistent with an age and origin similar to parallel actinolite + chlorite veins in the basalts.

Figure 22 shows that, as the contact is approached, maximum measured densities of vertical veins in the basalts increase, from 0.02 cm^{-1} at ≥1500 m from the contact to 0.14 cm^{-1} in the *actinolite + chlorite*

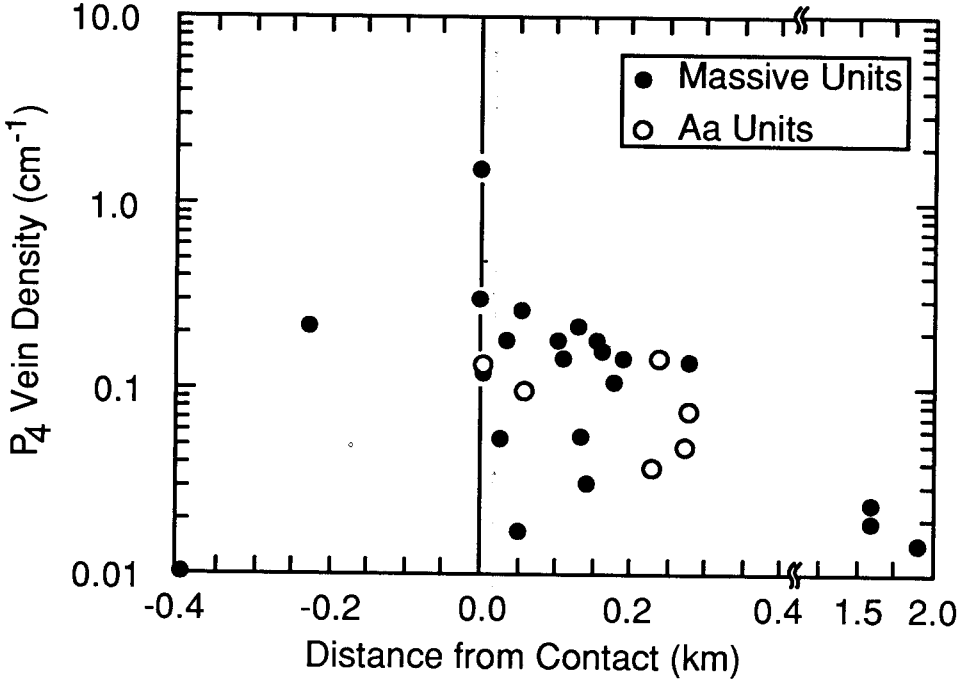

Fig. 22. Densities of all P_4 veins as a function of distance from the contact in the study area. Negative distances are in the Marginal Border Group gabbros of the Skaergaard intrusion, and positive distances are in the basalts. Note the break in the abscissa. See caption to figure 19 for distinction between massive and aa units.

zone, 0.25 cm^{-1} in the *pyroxene zone,* and 1.54 cm^{-1} in the *olivine zone.* In addition, P_4 vein densities in the gabbros also increase toward the contact (see also Bird, Rogers, and Manning, 1986). Thus, as with P_2 and P_3 structures, higher P_4 strains are recorded near the contact. Note that the distribution of strain contrasts with that recorded by P_2 structures in that there is no significant difference in P_4 vein density between massive and aa units (compare figs. 19 and 21). This suggests that mineral filling of the pore space eliminated mechanical differences between lithologies with different primary Φ^* by P_4 time.

P_5: quartz veins.—These pores postdate all other vein types in the study area. As shown in figure 14, virtually all quartz veins trend east-west. East-west faulting and dike emplacement continued in the region long after the Skaergaard magma-hydrothermal system had cooled to ambient conditions (Nielsen, 1978; Nielsen and others, 1981; Brooks and Nielsen, 1982b), and it is probable that quartz-filled veins and fault zones formed during development of these structures. These pore structures thus record the final return to the regional stress regime dominated by north-south σ_{min}.

Summary of Structural Evolution

Table 5 summarizes pore age groups and their inferred origin, and the migration of σ_{min} in the study area is summarized in figure 23. Prior to Skaergaard emplacement, regional least compressive stress was horizon-

TABLE 5

Origin and relative ages of pores

Relative age	Pore type(s)	Related event	σ_3
P_0	primary pores	extrusion and cooling of lavas	horizontal, north-south
P_1	pyroxene + oxide veins and north-south epidote + quartz veins	emplacement of north-south dikes	horizontal, east-west
P_2	horizontal veins, net veins, and hydrothermal breccias	pore fluid expansion due to heat transfer from crystallizing magma chamber	vertical >150 m from contact; random <150 m
P_3	quartz + feldspar veins in basalts and calcic amphibole veins in gabbros	contraction of Skaergaard gabbros shortly after crystallization	horizontal, east-west
P_4	east-west, northeast, and northwest veins including calcic amphibole + epidote + albite veins in basalts and gabbros, and epidote + quartz veins in basalts	emplacement of the Vandfaldsdalen macrodike and other mafic dikes	horizontal, northeast to northwest
P_5	quartz veins	faulting	horizontal, north-south

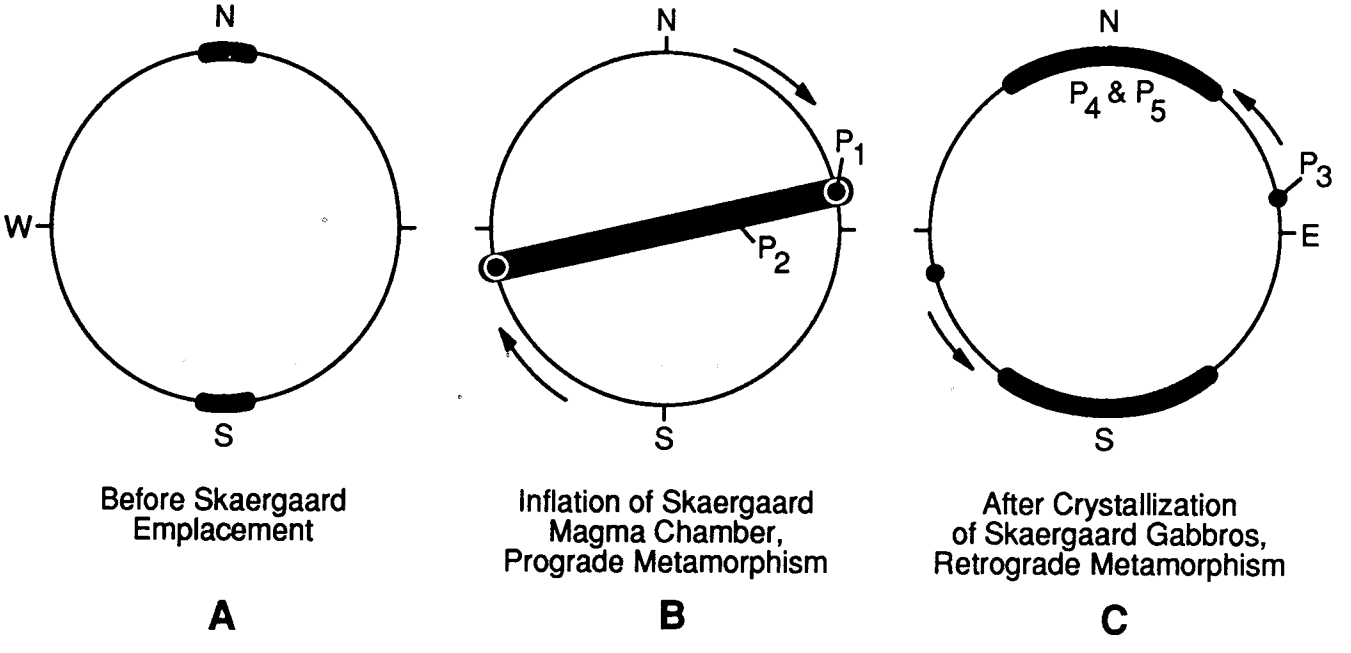

Fig. 23. Lower hemisphere equal area projections illustrating the migration of least compressive stress (σ_{min}) at the east contact of the Skaergaard intrusion. The range in orientations of σ_{min} is shown with the filled pattern for the pore age groups discussed in the text.

tal and oriented north-south (fig. 23A). The emplacement of the ~north-south dikes and formation of parallel P_1 fracture systems requires a nearly east-west σ_{min} (fig. 23B), marking the shift to a local stress regime. This may have occurred during the laccolithic stage of inflation of the Skaergaard magma chamber (Norton, Taylor, and Bird, 1984). Least compressive stress in the country rocks became vertical after the expanding magma chamber faulted and uplifted the overburden (fig. 23B). During the time in which the magma remained liquid it exerted pressure on the wall rocks to keep the chamber inflated, leading to maximum compressive stress oriented horizontal and normal to the contact. Heat transfer into the host rocks during this time caused pore fluid expansion, rock failure, and the formation of horizontal veins (P_2) along a thermal front migrating away from the contact. In the *pyroxene* and *olivine zones* near the contact, continued heating of pore fluids resulted in higher pore fluid pressures and led to repeated fracturing in a nearly isotropic stress regime in which local variations in σ_{min} resulted in net veins (P_2) with variable orientations. Because of their wide range and apparent randomness, orientations of σ_{min} in the *pyroxene* and *olivine zones* at this time are omitted from figure 23B. The volume decrease associated with crystallization of the magma was partly compensated by the formation of P_3 fractures. In the basalts, these structures were parallel to the contact and were filled by quartz + feldspar assemblages of both magmatic and hydrothermal origin. In the gabbros, P_3 veins were filled by calcic amphibole + pyroxene assemblages and were both parallel and normal to the contact. Subsequent fracturing was related to dike emplacement throughout the region, though strain continued to be concentrated near the basalt-gabbro contact. The orientations of P_4 and P_5 structures signify the return to a regional stress regime with σ_{min} oriented between north-northwest and northeast (fig. 23C).

PORE EVOLUTION AND FLUID FLOW

Comparison of Φ and Φ^*

Figure 24A compares measured Φ^* for the different pore age groups. The range in Φ^* for any pore type is a consequence of the variable distributions of the pores. For example, hydrothermal breccias have Φ^* of 12 percent, but they occur in only two zones (fig. 4), so most of the study area has hydrothermal breccia Φ^* of zero, and these values lie off the scale of figure 24A. The figure shows that the greatest Φ^* was associated with the earliest pores (P_0) and that, with the exception of P_1, maximum values of Φ^* associated with each pore group decrease with decreasing relative age. Since P_1 reflects porosity predating Skaergaard emplacement, this observation indicates that most of the strain recorded by secondary pores was generated shortly after gabbro emplacement.

The decrease in Φ^* implies that Φ of any representative rock volume near the Skaergaard's contact also decreased with time. Decreasing Φ with time was due to mineral filling of P_0 to P_4 structures rather than mechanical closure of pores with changes in stress regime, a conclusion

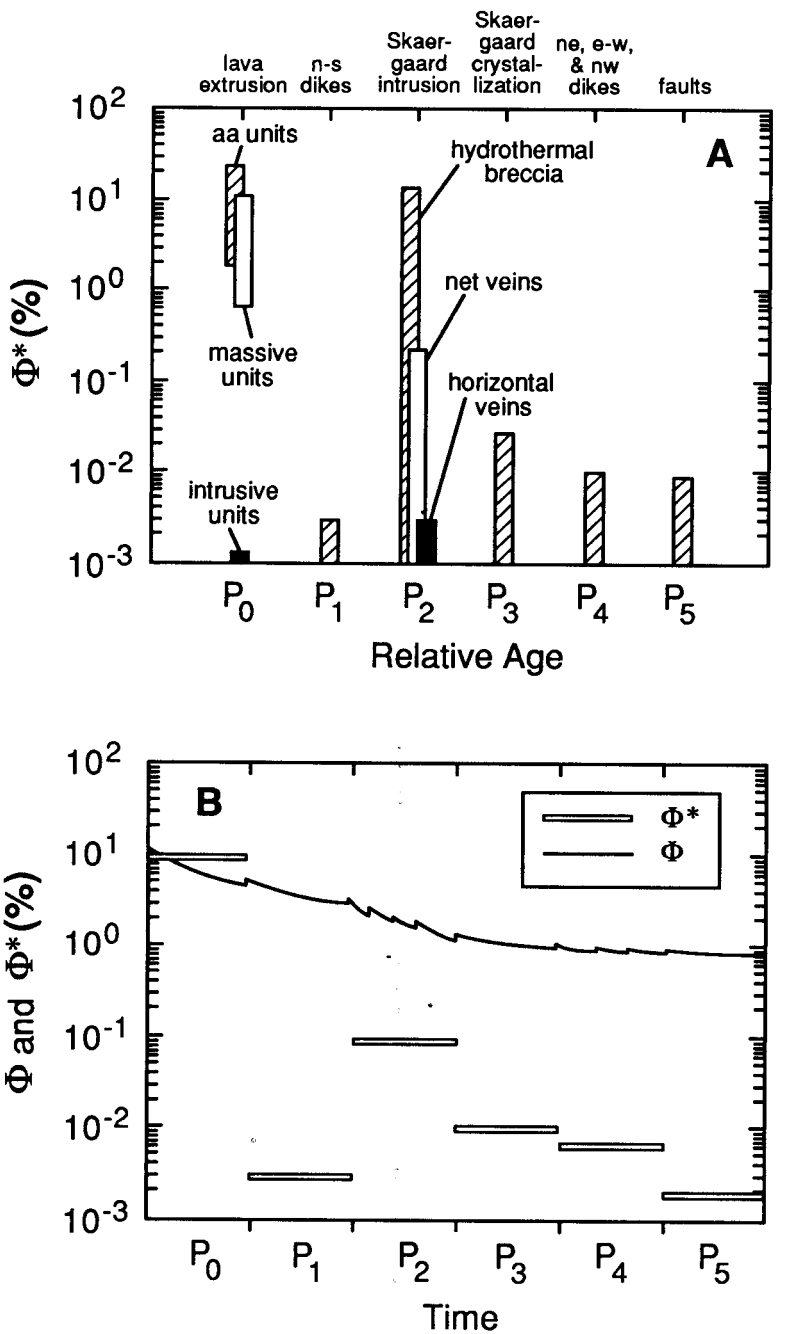

Fig. 24(A) Variation in Φ* with relative age during contact metamorphism. Relative age decreases to the right, and the structural or magmatic event associated with each pore age group is given at the top of the diagram. The different patterns are to ease distinction between Φ* of different pore types of the same relative age. Values of primary Φ* for intrusive units are zero but are shown on the diagram as having a maximum Φ* of $\sim 10^{-3}$ for the purposes of comparison with other pore types. Abbreviations: n-s, north-south; ne, northeast; e-w, east-west; nw, northwest. (B) Schematic comparison of the variation in Φ* and Φ with time for a hypothetical point in the *pyroxene zone* of the study area. Porosity (solid line) is a continuous function of time, whereas values of Φ* for the different pore age groups (open rectangles) are time invariant (see text). The abscissa is divided into equal times of formation of the pore age groups because, although certainly not equal, the actual durations of pore formation are not known.

supported by textures of pore-filling minerals. No brecciation or discontinuities were observed at centers of P_0 to P_4 pores (figs. 12 and 15). In addition, these pores commonly contain individual crystals which display optical continuity across the entire pore widths. Even if the stress regime changed before such pores were completely filled by secondary minerals, those crystals spanning the pore width might have acted as mineral bridges, keeping the pore open. Thus the difference between Φ and Φ^* for P_0 to P_4 is due to mineral filling of the pores. In contrast, P_5 pores display local brecciated textures and slickensided vein walls, suggesting that changes in stress regime or faulting may have modified Φ. However, although the differences between Φ and Φ^* for P_5 are more complex, this pore type is volumetrically insignificant and represents porosity that postdated the Skaergaard magma-hydrothermal system.

Figure 24B is a schematic illustration of the changes in Φ^* and Φ versus time for a hypothetical locality in the *pyroxene zone*. Note that Φ is a continuous function of time and that the abscissa of figure 24B is divided schematically into equal times of pore formation, because the actual durations are not known. This allows representation of a continuous variation in Φ with time as shown with the solid line in the figure. In contrast to Φ, Φ^* for each pore group is time invariant, because this variable represents the cumulative porosity produced during pore formation as measured at a single time of observation (see fig. 9). Values of Φ^* for the pore age groups are thus constant (open rectangles) over the respective times of pore formation.

The schematic evolution of porosity given in figure 24B shows initial Φ greater than Φ^* of primary pores ($\Phi^*_{P_0}$) immediately after lava extrusion. Values of Φ^* may underestimate Φ because Norton and Knapp (1977) found that porosities of 1 to 4 percent were associated with pores <1 mm in size, which was the detection limit for pores in the Φ^* measurement of the present investigation. However, this underestimate is likely to be minimal in rocks with large porosities such as basalts. For example, porosities of fresh vesicular basalts and basalt breccias from the Columbia River Plateau are respectively 5 and 10 percent (Atlantic Richfield Hanford Co., 1976). These values are virtually identical to mean Φ^* of 4 and 11 percent for the same lithologies in the Skaergaard's host basalts. With burial, the primary pores would have partially filled as secondary minerals precipitated from pore fluids. The subhedral textures of minerals filling primary pores indicate precipitation at least in part during prograde metamorphism. This requires the presence of unfilled primary pore space at the time of gabbro intrusion as is shown in figure 24B. Porosities of up to 40 percent have been measured in hydrothermally altered basalts by a variety of methods (Hyndman and Drury, 1976; Salisbury and others, 1977; Kirkpatrick, 1979; Becker and others, 1983; Jónsson and Stefánsson, 1982), suggesting that the persistence of open space even after burial to a depth of ~ 4 km is not unusual.

With the exception of the spatially restricted hydrothermal breccias, all secondary pore types have Φ^* less than 1 percent. Because it is likely

that the matrix Φ was about 1 percent or more (Norton and Knapp, 1977), Φ is shown in figure 24B to be greater than Φ^* values for all pore types formed after P_1. The first secondary pores formed when north-south dikes were emplaced, but these structures would have increased Φ by only a small amount. This is because even if all P_1 pores formed simultaneously such that Φ_{P_1} was equal to $\Phi^*_{P_1}$, the total P_1 porosity still would have been ≥ 3 orders of magnitude lower than the probable Φ_{P_0}. Deformation associated P_2 began when the Skaergaard magma was emplaced. The repeated cycles of pore pressure build-up, fracturing, and sealing, which led to the net-vein textures, would have caused the variation in Φ schematically shown in figure 24B for the P_2 time interval. Pores of P_3 age formed at the time of, or shortly after, gabbro crystallization and probably reflect strain concentrated over a relatively short time interval (fig. 24B). In contrast, P_4 and P_5 veins in the basalts formed during emplacement of dikes whose variable orientations suggest intrusion at different times in response to different stress regimes. This would result in changes in Φ with time that were similar to those associated with P_2. The change in Φ with time implied by figure 24B suggests that the greatest quantity of hydrothermal fluid resided in the rocks early in the system's history during prograde metamorphism.

Φ^* *and the Evolution of Fluid Flow*

Figure 24B shows that the matrix porosity represents a much larger component of total Φ than secondary porosity (P_1–P_5). However, because ≥ 90 percent of the matrix pores in fractured media are residual pores (Norton and Knapp, 1977), the well-connected pore networks of P_1 to P_5 were likely to have been a major component of the system's flow porosity. Thus, despite their relatively small contribution to the total porosity, P_1 to P_5 pores are the most important structures for understanding the evolution of fluid flow.

The evolution of porosity and fluid flux vectors are constrained by the identified pore types are shown in figure 25. Prior to the intrusion of the Skaergaard magma, north-northwest- to north-south-trending fractures formed and were filled by basaltic magma and hydrothermal fluids (fig. 25A). Flux vectors of hydrothermal fluids within these fractures probably had a predominantly vertical component. After emplacement of the Skaergaard magma, temperatures increased in the aureole and caused outward migration of both metamorphic mineral zones and a deformation front marked by horizontal vein formation (fig. 25B and C). When maximum temperatures were attained, the front of horizontal vein formation had reached its greatest distance east of the contact (~ 400 m). Temperature-induced density gradients in the pore fluids caused fluid migration toward the heat source (Norton and Taylor, 1979; Manning, ms). The lack of vertical connectivity of horizontal veins at this time confined fluids in the pore network beyond ~ 150 m to bedding-parallel zones, including high-primary-Φ^* horizons such as aa flows and net-

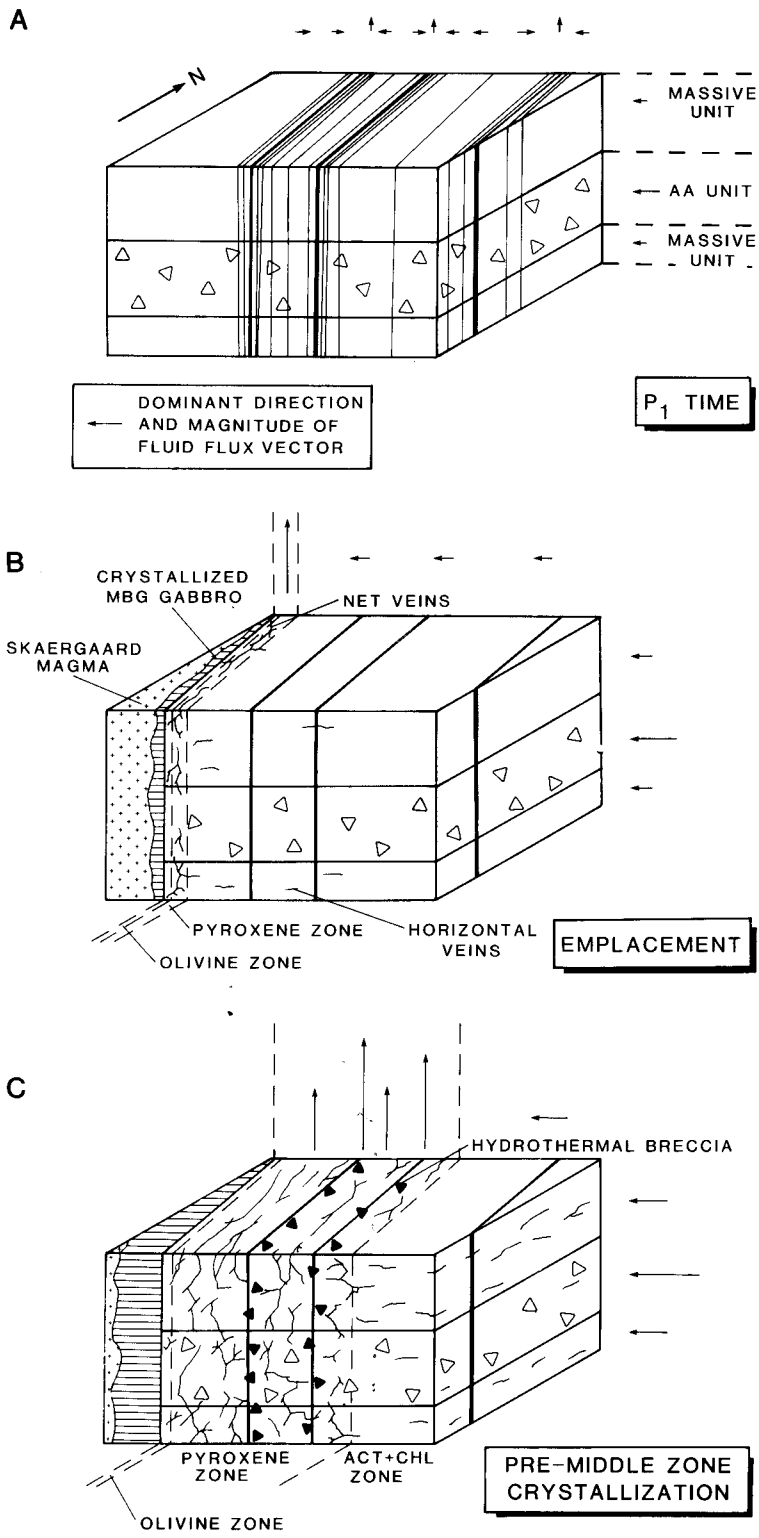
A
N
MASSIVE UNIT
AA UNIT
MASSIVE UNIT
DOMINANT DIRECTION AND MAGNITUDE OF FLUID FLUX VECTOR
P1 TIME
B
CRYSTALLIZED MBG GABBRO
NET VEINS
SKAERGAARD MAGMA
PYROXENE ZONE
HORIZONTAL VEINS
OLIVINE ZONE
EMPLACEMENT
C
HYDROTHERMAL BRECCIA
PYROXENE ZONE
ACT+CHL ZONE
OLIVINE ZONE
PRE-MIDDLE ZONE CRYSTALLIZATION

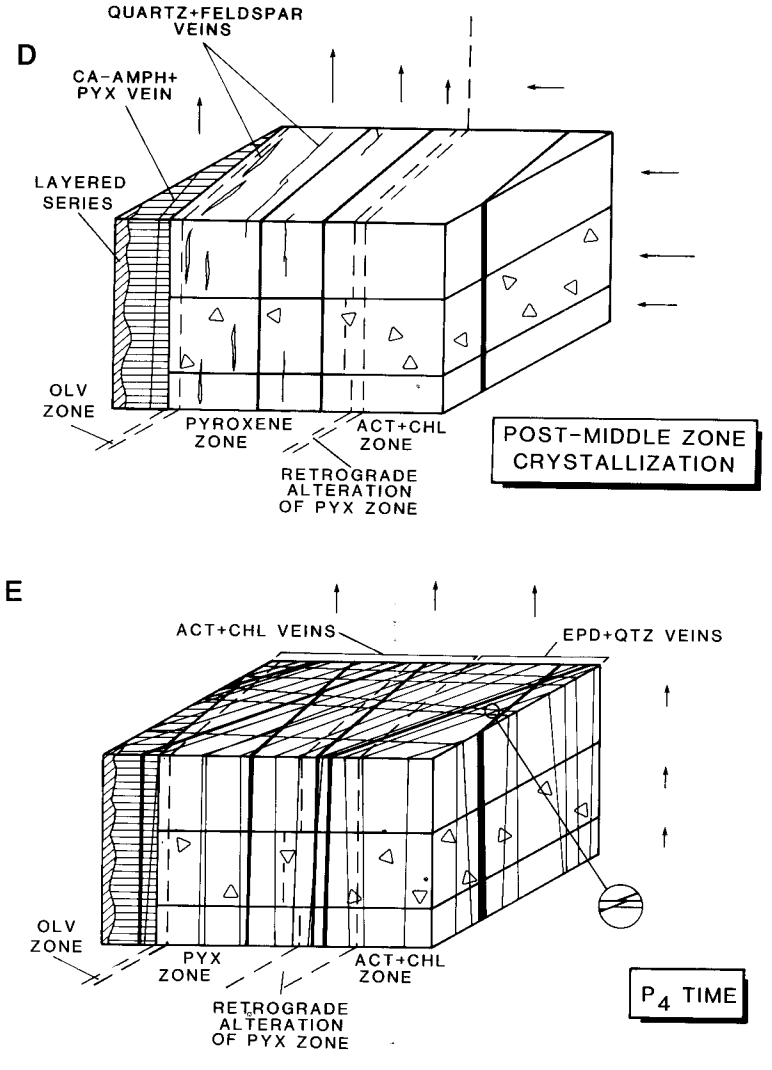

Fig. 25. Schematic block diagrams showing structural and pore evolution at the east contact of the Skaergaard magma-hydrothermal system. Arrows are fluid path lines, and their lengths qualitatively depict relative magnitudes of fluid flux. The filled, planar features are dikes. Note that each diagram shows only the pores formed during the stated time period for simplicity. The inset to (E) shows that northeast trending P_4 veins crosscut and are crosscut by east-west P_4 veins.

works of P_0 connected by horizontal P_2 veins in vesicular flows. The higher porosities and greater potential for pore connectivity in aa flows led to higher magnitudes of fluid flux than in vesicular flows (Manning, ms; Manning and Bird, 1991), similar to the near-surface hydrology of

recent volcanic terranes such as Hawaii (Stearns and Vaksvik, 1935; Stearns, 1940, 1942; Stearns and Macdonald, 1946, 1947). Because of their low $\Phi^*_{P_0}$, the north-south dikes may have initially been impermeable to lateral fluid flow, but these lithologies are commonly crosscut by dense P_2 networks (fig. 12C) which would have allowed fluid migration through them after Skaergaard emplacement. However, the presence of magma in the chamber created an impermeable barrier, and fluids migrating toward the heat source were deflected upward near the contact (Norton and Taylor, 1979). The increased vertical connectivity of P_2 net veins and hydrothermal breccias within 150 m of the contact (fig. 20) were the structures that allowed this vertical fluid flow. In particular, the relatively high porosities of the breccias along dike margins provided the conduits for potentially large magnitudes of upward fluid flux. This is consistent with the observation that highly fractured dikes and dike margins represent excellent aquifers in near-surface environments (Adyalkar and Mani, 1974; Morel and Wikamaratna, 1982; Boonstra and Boehmer, 1986; Boehmer and Boonstra, 1987).

The decrease in volume of the intrusion upon magma crystallization apparently led to the formation of the early calcic amphibole + pyroxene veins in the Marginal Border Group and the quartz + feldspar veins in the basalts (fig. 25D). Local retrograde alteration of the *pyroxene zone* occurred as temperatures declined and cool hydrothermal fluids migrated inward through primary pores and horizontal veins. Vertical P_4 and P_5 fractures mark the return to the regional stress regime with σ_{min} oriented horizontal between north-northwest and northeast, consistent with the orientations of later mafic dikes (fig. 25E). All pores that formed after crystallization of the gabbro were vertical and provided conduits that allowed continued vertical migration of fluids. Because they postdate crystallization of the Skaergaard, the P_3 and P_4 structures were the channels for the fluids that entered the intrusion and caused high-temperature mineralogic and ^{18}O alteration of the gabbros.

These results show that the abundance and distribution of primary porosity is of central importance of the early stages of fluid flow during contact metamorphism. The strong porosity contrasts in the different map units of the study area resulted in a contrasting behavior of the different lithologies shortly after Skaergaard emplacement: fluid pressure build-up in isolated pores in massive units caused rock failure, generating the porosity allowing fluid flow; whereas in aa units, primary flow porosity as sufficient to allow increases in fluid pressure to be dissipated by flow. Each contact metamorphic environment will have a unique distribution of primary porosity that is a function of the lithologies present and the previous geologic history. Consequently, understanding the initial conditions for fluid flow requires determination of the nature of primary porosity in the aureole of interest.

In addition, the orientation and abundance of secondary pores reflect the interdependence of the state of stress, permeability, mineral

reactions, and fluid density. These parameters govern the processes of heat transport, fluid expansion, rock failure, fluid flow, and pore filling, and the resulting pore network shows how these processes interact during the dissipation of the magmatic thermal anomaly. The abundance and orientation of pore structures will be unique in each contact metamorphic environment, but in every case, the pore network will provide the record of the changes in stress, permeability, mineral reactions, and fluid density with time that allows a more detailed understanding of fluid migration during contact metamorphism in the system of interest.

Acknowledgments

This paper represents a portion of the senior author's Ph.D. thesis at Stanford University. We thank B. Yardley and D. Norton for insightful reviews of the manuscript and C. K. Brooks, R. J. Nevle, T. F. D. Nielsen, J. Olsen, A. Rubin, N. M. Rose, and M. Rosing for helpful discussions. Financial support was provided by NSF grants 84-18129, 86-06256, 88-03754 to D. K. Bird and 86-15714 to S. R. Bohlen, as well as by the Geological Society of America, a Corning Glass Science fellowship, the Shell Companies, and the McGee Trust. We also thank R.A. Gannicott of Platinova Resources, Ltd., and the Geological Survey of Greenland for field support.

References

Adyalkar, P. G., and Mani, V. V. S., 1974. Application of groundwater hydraulics to a basaltic water table aquifer: Journal of Hydrology, v. 25, p. 211–218.

Atlantic Richfield Hanford Company, 1976, Preliminary feasibility study of storage of radioactive wastes in Columbia River basalts: Richland, Washington, Atlantic Richfield Hanford Company, ARH-ST-137, v. 1, 168 p.

Barton, C. C., and Hsieh, P. A., 1989, Physical and hydrologic-flow properties of fractures; Washington, D. C., American Geophysical Union, International Geological Congress, 28th, Field Trip Guidebook T385, 36 p.

Becker, K., Langseth, M. G., von Herzen, R. P., and Anderson, R. N., 1983, Deep crustal geothermal measurements, hole 504B, Costa Rica rift: Journal of Geophysical Research, v. 88, p. 3447–3457.

Bianchi, L., and Snow, D. T., 1969, Permeability of crystalline rocks interpreted from measured orientations and apertures of fractures: Jodphur, Rajastan, Arid Zone Research Association of India, Annals of Arid Zone, v. 8, p. 231–245.

Bird, D. K., Manning, C. E., and Rose, N. M., 1988, Hydrothermal alteration of Tertiary layered gabbros, East Greenland: American Journal of Science, v. 288, p. 405–457.

Bird, D. B., Rogers, R. D., and Manning, C. E., 1986, Mineralized fracture systems of the Skaergaard intrusion: Meddelelser om Grønland, Geoscience, v. 16, 68 p.

Bird, D. K., Rosing, M. T., Manning, C. E., and Rose, N. M, 1985, Geologic field studies of the Miki Fjord area, East Greenland: Bulletin of the Geological Society of Denmark, v. 34, p. 219–236.

Boehmer, W. K., and Boonstra, J., 1987, Analysis of drawdown in the country-rock of composite dike aquifers: Journal of Hydrology, v. 94, p. 199–214.

Boonstra, J., and Boehmer, W. K., 1986, Analysis of data from aquifer and well tests in intrusive dikes: Journal of Hydrology, v. 88, p 301–317.

Brooks, C. K., 1979, Geomorphological observations at Kangerdlugssuaq, East Greenland: Meddelelser om Grønland, Geoscience, v. 1, 21 p.

———— 1980, Episodic volcanism, epeirogenesis and the formation of the North Atlantic ocean: Paleogeography, Paleoclimatology, Paleoecology, v. 30, p. 229–242.

Brooks, C. K., and Gleadow, A. J. W., 1979, A fission-track age for the Skaergaard intrusion and the age of the East Greenland basalts: Geology, v. 5, p. 539–540.

Brooks, C. K., and Nielsen, T. F. D., 1978, Early stages of the differentiation of the Skaergaard magma as revealed by a closely related suite of dike rocks: Lithos, v. 11, p. 1–14.

———— 1982a, The East Greenland continental margin: a transition between oceanic and continental magmatism: Journal of the Geological Society of London, v. 139, p. 265–275.

———— 1982b, The Phanerozoic development of the Kangerdlugssuaq area, East Greenland: Meddelelser om Grønland, Geoscience, v. 9, 30 p.

Chayes, F., 1956, Petrographic model analysis: an elementary statistical appraisal: New York, John Wiley & Sons, 113 p.

Deer, W. A., 1976, Tertiary igneous rocks between Scoresby Sund and Kap Gustav Holm, East Greenland, *in* Escher, A., and Watt, W. S., eds., Geology of Greenland: Copenhagen, The Geological Survey of Greenland, p. 405–429.

Delaney, P. T., 1982, Rapid intrusion of magma into wet rock: groundwater flow due to pore pressure increases: Journal of Geophysical Research, v. 87, p. 7739–7756.

Delaney, P. T., and Pollard, D. D., 1981, Deformation of host rocks and flow of magma during growth of minette dikes and breccia-bearing intrusions near Ship Rock, New Mexico: U. S. Geological Survey Professional Paper 1202, 61 p.

Delaney, P. T., Pollard, D. D., Ziony, J. I., and McKee, E. H., 1986, Field relations between dikes and joints: emplacement processes and paleostress analysis: Journal of Geophysical Research, v. 91, p. 4920–4938.

Douglas, J. A. V., 1964, Geological investigations in East Greenland. VII. The Basistoppen sheet, a differentiated basic intrusion into the upper part of the Skaergaard complex: Meddelelser om Grønland, v. 164, 66 p.

Ferry, J. M., 1987, Metamorphic hydrology at 13-km depth and 400–550°C: American Mineralogist, v. 72, p. 39–58.

———— 1988, Contrasting mechanisms of fluid flow through adjacent stratigraphic units during regional metamorphism, south-central Maine, USA: Contributions to Mineralogy and Petrology, v. 98, p. 1–12.

———— 1989, Contact metamorphism of roof pendants at Hope Valley, Alpine County, California, USA. A record of the hydrothermal system of the Sierra Nevada Batholith: Contributions to Mineralogy and Petrology, v. 101, p. 402–417.

Ferry, J. M., Mutti, L. J., and Zuccala, G. J., 1987, Contact metamorphism/hydrothermal alteration of Tertiary basalts from the Isle of Skye, northwest Scotland: Contributions to Mineralogy and Petrology, v. 95, p 166–181.

Haynes, F. M., and Titley, S. R., 1980, The evolution of fracture-related permeability within the Ruby Star granodiorite. Sierrita Porphyry Copper Deposit, Pima County, Arizona: Economic Geology v. 75, p. 673–683.

Helgeson, H. C., and Kirkham, 1974, Theoretical prediction of the thermodynamic behavior of aqueous electrolytes at high pressures and temperatures: I. summary of the thermodynamic/electrostatic properties of the solvent: American Journal of Science, v. 274, p. 1089–1198.

Hirschmann, M., 1987, Rb-Sr age and origin of the transgressive granophyres of the Skaergaard intrusion: Eos, v. 68, p. 1518.

———— 1988, Petrogenesis of the transgressive granophyres from the Skaergaard intrusion, East Greenland: Geological Society of America Abstracts with Programs, v. 20, no. 7, p. A156.

Holness, M. B., Bickle, M. J., and Harte, B., 1989. Textures of forsterite-calcite marbles from the Beinn an Dubhaich aureole, Skye, and implications for the structure of metamorphic porosity: Journal of the Geological Society of London, v. 146, p. 917–920.

Hoover, J. D., 1989a, Petrology of the Marginal Border Series of the Skaergaard intrusion: Journal of Petrology, v. 30, p. 399–439.

———— 1989b, The chilled marginal gabbro and other contact rocks of the Skaergaard intrusion: Journal of Petrology, v. 30, p. 441–476.

Hover-Granath, V. C., Papike, J. J., and Labotka, T. C., 1983. The Notch Peak contact metamorphic aureole, Utah: petrology of the Big Horse Limestone Member of the Ore Formation: Bulletin of the Geological Society of America, v. 94, p. 889–906.

Hyndman, R. D., and Drury, M. J., 1976, The physical properties of oceanic basement rocks from deep drilling on the mid-Atlantic ridge: Journal of Geophysical Research, v. 81, p. 4042–4052.

Jónsson, G., and Stefánsson, V., 1982, Density and porosity logging in the IRDP hole, Iceland: Journal of Geophysical Research, v. 87, p 6619–6630.

Kays, M. A., Goles, G. G., and Grover, T. W., 1989, Precambrian sequence bordering the Skaergaard intrusion: Journal of Petrology, v. 30, p. 321–361.
Kirkpatrick, R. J., 1979, The physical state of the oceanic crust: results of the downhole geophysical logging in the mid-Atlantic ridge at 23°N: Journal of Geophysical Research, v. 84, p. 178–188.
Knapp, R. B., and Knight, J. E., 1977, Differential thermal expansions of pore fluids: fracture propagation and microearthquake production in hot pluton environments: Journal of Geophysical Research, v. 82, p. 2515–2522.
Knapp, R. B., and Norton, D., 1981, Preliminary numerical analysis of processes related to magma crystallization and stress evolution in cooling pluton environments: American Journal of Science, v. 281, p. 35–68.
Larsen, L. M., and Watt, W. S., 1985, Episodic volcanism during break-up of the North Atlantic: evidence from the East Greenland plateau basalts: Earth and Planetary Science Letters, v. 73, p. 105–116.
Leeman, W. P., Dasch, E. J., and Kays, M. A., 1976, $^{207}Pb/^{206}Pb$ whole-rock age of gneisses from the Kangerdlugrssuaq area, eastern Greenland: Nature, v. 263, p. 469–471.
Macdonald, G. A., 1967, Forms and structures of extrusive basaltic rocks, *in* Hess, H. H., and Poldervaart, A., editors, Basalts: New York, John Wiley & Sons, p. 1–61.
Manning, C. E., ms., 1989, Porosity evolution, contact metamorphism, and fluid flow in the host basalts of the Skaergaard magma-hydrothermal system: Ph.D. thesis, Stanford University, Stanford, California, 190 p.
Manning, C. E., and Bird, D. K., 1986, Hydrothermal clinopyroxenes of the Skaergaard intrusion: Contributions to Mineralogy and Petrology, v. 92, p. 437–447.
———— 1987, Wollastonite + fluorite in metabasalt host rocks of the Skaergaard intrusion: implications for metamorphic fluid composition: Geological Society of America Abstracts with Programs, v. 19, no. 7, p. 759.
———— 1990, Fluorian garnets from the host rocks of the Skaergaard intrusion: implications for metamorphic fluid composition: American Mineralogist, 75, p. 859–873.
———— 1991, Contact metamorphism and water-rock interaction in the Skaergaard intrusion host basalts: in preparation.
McBirney, A. R., 1989, The Skaergaard Layered Series: I. Structure and average compositions: Journal of Petrology, v. 30, p. 363–397.
McBirney, A. R., and Noyes, R. M., 1979, Crystallization and layering of the Skaergaard intrusion: Journal of Petrology, v. 30, p 487–564.
Morel, E. H., and Wikamaratna, R. S., 1982, Numerical modelling of groundwater flow in regional aquifers dissected by dikes: Hydrological Sciences Journal, v. 27, p. 63–77.
Moskowitz, B., and Norton, D., 1977, A preliminary analysis of intrinsic fluid and rock resistivity in active hydrothermal systems: Journal of Geophysical Research, v. 82, p 5787–5795.
Myers, J. S., 1978, Skaergaard intrusion, East Greenland: contact metamorphism and deformation on Mellemo: Bulletin of the Geological Society of Denmark, v. 28, p. 1–4.
Nabelek, P. I., Labotka, T. C., O'Neil, J. R., and Papike, J. J., 1984, Contrasting fluid/rock interaction between the Notch Peak granitic intrusion and argillites and limestones in western Utah: evidence from stable isotopes and phase assemblages: Contributions to Mineralogy and Petrology, v. 86, p. 25–34.
Naslund, H. R., 1984, Petrology of the Upper Border Series of the Skaergaard intrusion: Journal of Petrology, v. 25, p. 185–212.
———— 1986, Disequilibrium partial melting and rheomorphic layer formation in the contact aureole of the Basistoppen sill, East Greenland: Contributions to Mineralogy and Petrology, v. 93, p. 359–367.
———— 1989, Petrology of the Basistoppen sill, East Greenland: a calculated magma differentiation trend: Journal of Petrology, v. 30, p. 299–319.
Nehlig, P., and Juteau, T., 1988, Flow porosities, permeabilities and preliminary data of fluid inclusions and fossil thermal gradients in the crustal sequence of the Semail ophiolite (Oman): Tectonophysics, v. 151, p. 199–221.
Nielsen, T. F. D., 1978, The Tertiary dike swarms of the Kangerdlugssuaq area, East Greenland. An example of magmatic development during continental break-up: Contributions to Mineralogy and Petrology, v. 67, p 63–78.
Nielsen, T. F. D., Soper, N. J. Brooks, C. K. Faller, A. M., Higgens, A. C., and Matthews, D. W., 1981, The pre-basaltic sediments and the lower basalts at Kangerdlugssuaq, East Greenland, their statigraphy, lithology, palaeomagnetism and petrology: Meddelelser om Grønland, Geoscience, v. 6, 25 p.

Noble, R. H., Macintyre, R. M., and Brown, P. E., 1988, Age constraints on Atlantic evolution: timing of magmatic activity along the East Greenland continental margin, *in* Morton and Parsons, eds., Early Tertiary Volcanism and the Opening of the North Atlantic: Geological Society of London Special Publication 39, p. 201–214.

Norton, D., 1979, Transport phenomena in hydrothermal systems: the redistribution of chemical components around cooling magmas: Bulletin de Minéralogie, v. 102, p. 471–486.

———— 1984, Theory of hydrothermal systems: Annual Review of Earth and Planetary Sciences, v. 12, p. 155–177.

Norton, D., and Knapp, R., 1977, Transport phenomena in hydrothermal systems: the nature of porosity: American Journal of Science, v. 277, p. 913–936.

Norton, D., and Knight, J. E., 1977, Transport phenomena in hydrothermal systems: cooling plutons: American Journal of Science, v. 277, p. 937–981.

Norton, D., and Taylor, H. P., Jr., 1979, Quantitative simulation of the hydrothermal systems of crystallizing magmas on the basis of transport theory and oxygen isotope data: an analysis of the Skaergaard intrusion: Journal of Petrology, v. 20, p. 421–486.

Norton, D., Taylor, H. P., Jr., and Bird, D. K., 1984, The geometry and high temperature brittle deformation of the Skaergaard intrusion: Journal of Geophysical Research, v. 89, p. 10178–10192.

Ramsey, J. G., 1980, The crack-seal mechanism of rock deformation: Nature, v. 284, p. 135–139.

Rogers, R. D., and Bird, D. K., 1987, Fracture propagation associated with dike emplacement at the Skaergaard intrusion, East Greenland: Journal of Structural Geology, v. 9, p. 71–86.

Rosing, M. T., Lesher, C., and Bird, D. K., 1989, Chemical modification of East Greenland Tertiary magmas by two-liquid interdiffusion: Geology, v. 17, p. 625–629.

Salisbury, M. H., Stephan, R. T., Christensen, N. I., Francheteau, J., Hamano, Y., Hobart, M., and Johnson, D., 1979, The physical state of the upper levels of Cretaceous oceanic crust from the results of logging, laboratory studies and oblique seismic experiment at DSDP sites 417 and 418, *in* Talwani, M., and others, editors, Deep Drilling Results in the Atlantic Ocean: Washington, D. C., American Geophysical Union, v. 2, p. 113–134.

Snow, D. T., 1968, Rock fracture spacings, openings, and porosities: Journal of the Soil Mechanics and Foundations Division of the American Society of Civil Engineers, v. 94, p. 73–91.

———— 1970, The frequency and apertures of fractures in rock: International Journal of Rock Mechanics and Mining Sciences, v. 7, p. 23–40.

Soper, N. J., Downie, C., Higgins, A. C., and Costa, L. I., 1976b, Biostratigraphic ages of Tertiary basalts on the East Greenland continental margin and their relationship to plate separation in the northeast Alantic: Earth and Planetary Science Letters, v. 32, p. 149–157.

Soper, N. J., Higgins, A. C., Downie, C., Matthews, D. W., and Brown, P. E., 1976a, Late Cretaceous-Tertiary stratigraphy of the Kangerdlugssuaq area, East Greenland, and the age of the opening of the north-east Atlantic: Journal of the Geological Society of London, v. 132, p. 85–104.

Stearns, H. T., 1940, Geology and ground-water resources of the islands of Lanai and Kahoolawe, Hawaii: Hawaii Division of Water and Land Management Bulletin, v. 6, 173 p.

———— 1942, Hydrology of lava-rock terranes, *in* Meinzer, O. E., ed., Hydrology: New York, McGraw-Hill, p. 678–703.

Stearns, H. T., and Macdonald, G. A., 1946, Geology and ground-water resources of the island of Hawaii: Hawaii Division of Water and Land Management Bulletin, v. 9, 363 p.

———— 1947, Geology and ground-water resources of the island of Molokai, Hawaii: Hawaii Division of Water and Land Management Bulletin, v. 11, 113 p.

Stearns, H. T., and Vaksvik, K. N., 1935, Geology and ground-water resources of the island of Oahu, Hawaii: Hawaii Division of Water and Land Management Bulletin, v. 1, 479 p.

Taylor, H. P., Jr., and Forester, R. W., 1979, An oxygen isotope study of the Skaergaard intrusion and its country rocks: a description of a 55-m.y. old fossil hydrothermal system: Journal of Petrology, v. 20, p. 355–419.

Titley, S. R., Thompson, R. C., Haynes, F. M., Manske, S. L., Robison, L. C., and White, J. L., 1986, Evolution of fractures and alteration in the Sierrita-Esperanza hydrothermal system, Pima County, Arizona: Economic Geology, v. 81, p. 343–370.

Villas, R. N., and Norton, D., 1977, Irreversible mass transfer between circulating hydrothermal fluids and the Mayflower stock: Economic Geology, v. 72, p. 1471–1504.

Wager, L. R., 1934, Geological investigations in East Greenland. I. General geology from Angmagsalik to Kap Dalton: Meddelelser om Grønland, v. 105, 46 p.

———— 1947, Geological investigations in East Greenland. IV. The Stratigraphy and tectonics of Knud Rasmussens Land and the Kangerdlugssuak region: Meddeleser om Grønland, v. 5, 64 p.

Wager, L. R., and Brown, G. M., 1967, Layered Igneous Rocks: San Francisco, W. H. Freeman, 588 p.

Wager, L. R., and Deer, W. A., 1938, A dyke swarm and crustal flexture in East Greenland: Geological Magazine, v. 75, p. 39–46.

———— 1939, Geological investigations in East Greenland. III. The petrology of the Skaergaard intrusion, Kangerdlugssuak region: Meddelelser om Grønland, v. 134, 352 p.

Walder, J., and Nur, A., 1984, Porosity reduction and crustal pore pressure development: Journal of Geophysical Research, v. 89, p. 11539-11.